Flexoelectric control of physical properties by atomic force microscopy

Cite as: Appl. Phys. Rev. **8**, 041327 (2021); https://doi.org/10.1063/5.0067429
Submitted: 16 August 2021 • Accepted: 18 November 2021 • Published Online: 29 December 2021

Sung Min Park, Bo Wang, Long-Qing Chen, et al.

Applied Physics Reviews REVIEW scitation.org/journal/are

Flexoelectric control of physical properties by atomic force microscopy

Cite as: Appl. Phys. Rev. 8, 041327 (2021); doi: 10.1063/5.0067429
Submitted: 16 August 2021 · Accepted: 18 November 2021 ·
Published Online: 29 December 2021

Sung Min Park,[1,2] Bo Wang,[3] Long-Qing Chen,[3] Tae Won Noh,[1,2] Sang Mo Yang,[4,a)] and Daesu Lee[5,a)]

AFFILIATIONS

[1]Center for Correlated Electron Systems, Institute for Basic Science (IBS), Seoul 08826, South Korea
[2]Department of Physics and Astronomy, Seoul National University, Seoul 08826, South Korea
[3]Department of Materials Science and Engineering, The Pennsylvania State University, University Park, Pennsylvania 16802, USA
[4]Department of Physics, Sogang University, Seoul 04107, South Korea
[5]Department of Physics, Pohang University of Science and Technology (POSTECH), Pohang 37673, South Korea

[a)]Authors to whom correspondence should be addressed: smyang@sogang.ac.kr and dlee1@postech.ac.kr

ABSTRACT

The past decade has witnessed the tremendous scientific and technological potential of nanoscale flexoelectricity in solids. The flexoelectric effect describes the universal generation of electric polarization in response to strain gradients and could be inversely enhanced at reduced nanoscale dimensions. Based on this unique scaling effect, nanoscale flexoelectricity has shown exciting physical phenomena, promising novel electronic, electromechanical, and photovoltaic applications. One of the most powerful ways to harness nanoscale flexoelectricity is to press the surface of a material through an atomic force microscope (AFM) tip to generate large strain gradients. This so-called AFM tip pressing allows us to locally break the inversion symmetry in any materials and study all the fascinating physical phenomena associated with inversion asymmetry. Although this technique has recently facilitated many important studies on nanoscale flexoelectricity, its effective use still requires a more solid foundation. In this review, we provide a comprehensive guideline to exploring nanoscale flexoelectricity via AFM tip pressing. We also discuss recent progress and the future research direction of AFM tip pressing-driven nanoscale flexoelectricity.

TABLE OF CONTENTS

I. INTRODUCTION

The development of scanning probe microscopy (SPM) has significantly enlarged our understanding of various physical and chemical phenomena that occur at the nano- and atomic scales. The realization of scanning tunneling microscopy[1] and atomic force microscopy (AFM)[2] has enabled the real-space imaging of surface morphology at atomic resolution. In addition, these techniques have allowed the detection of local material responses against external stimuli, leading to the development of many SPM modes. For example, piezoresponse force microscopy (PFM) detects the surface oscillation induced by the applied ac voltage, that is, the converse piezoresponse of the sample.[3–5] Also, conductive-AFM measures the local current flowing between the tip and the sample under the applied bias.[6] Beyond the measurements of topography and material responses, the active manipulation of material properties using the AFM tip has also been extensively conducted.

In the context of active manipulation, AFM tip pressing is a simple but highly effective way to perturb the material properties. Pressing the surface of a sample using a sharp AFM tip with relatively larger loading forces of several μN [i.e., compared to those (a few tens of nN) usually used for topography imaging] can create substantial elastic deformation beneath the tip. A large strain gradient forms near the elastically deformed contact region, naturally breaking the inversion symmetry. The induced inversion asymmetry can modulate various physical properties due to the coupling to order parameters, such as polarization and magnetization.[7–10]

Regarding the inversion symmetry breaking coupled with other order parameters, flexoelectricity has recently been attracting much interest. Flexoelectricity describes the universal generation of electric polarization under strain gradient (direct effect)[11] or the mechanical response caused by an electric field gradient (converse effect).[12–17] Flexoelectricity can be phenomenologically expressed as

$$P_l = \mu_{ijkl}\frac{\partial \varepsilon_{ij}}{\partial x_k}, \tag{1}$$

where P_l is the generated polarization, μ_{ijkl} the flexoelectric coefficient (a fourth-rank polar tensor), ε_{ij} the strain component, x_k the position coordinate, and $\partial\varepsilon_{ij}/\partial x_k$ the strain gradient component. From Eq. (1), it is intuitively apparent that there are two key features of flexoelectricity: the unique scaling effect and the inversion symmetry-breaking effect. Since strain gradients are inversely proportional to the length scale, they could become tremendously enhanced at reduced nanoscale dimensions. Moreover, as strain gradients universally break the inversion symmetry, flexoelectricity appears in all materials with any crystal symmetries, including dielectrics[18,19] to semiconductors[20–22] and biomaterials[23,24] to two-dimensional materials.[25] Due to this ubiquitous effect, flexoelectricity might hold advantages over piezoelectricity that exists in only 20 point groups of all 32 point groups.

AFM tip pressing has recently proven to be a highly effective approach to exploit the two unique features of flexoelectricity. Using the AFM tip, it is possible to select a location and vary the applied force systematically to probe the material's responses at the nanoscale. The radius of an AFM tip is typically several tens of nanometers, which is beneficial for fully exploiting the enhanced effects of flexoelectricity at reduced nanoscale dimensions. Furthermore, the AFM tip-induced local breaking of the inversion symmetry can tune various physical properties and reveal hitherto hidden emergent phenomena.

There are several excellent reviews on flexoelectricity.[26–31] However, despite recent significant advances in this research area, there has to date been no focused review on nanoscale flexoelectricity explored by AFM tip pressing.[32] There are still some challenges to be overcome. First, the interpretation of experimental data requires special attention. Under AFM tip pressing, not only flexoelectricity but also other effects (such as piezoelectricity, Vegard strain effect, piezochemical effect, and triboelectricity) can play a role in the experimental observations. Second, since the AFM tip-induced strain gradient is a rather complex quantity to measure accurately, there should be adequate guidelines for estimating the strain gradient based on an appropriate theoretical model. In this review, after presenting a brief history of flexoelectricity in solids (Sec. II), we discuss relevant effects resulting from AFM tip pressing (Sec. III) and provide general guidance on using this technique (Sec. IV). Next, we discuss recent progress (Sec. V) and future direction of research (Sec. VI) of AFM-controlled nanoscale flexoelectricity.

II. A BRIEF HISTORY OF FLEXOELECTRICITY IN SOLIDS

The concept of flexoelectricity was first developed in the 1960s,[11,33] and the phenomenon was given the name "flexoelectricity" in 1981.[34] After a while, systematic theoretical descriptions of flexoelectricity in solids have been suggested from the 1980s,[35] and the microscopic models have been further provided since the late 2000s.[36–40] Meanwhile, the flexoelectric coefficients μ_{ijkl} of bulk solids were experimentally measured in 2007[18] and were found to be small (typically, ranging from 10^{-6} to 10^{-10} C m^{-1}).[39,41–43] Elastic deformation is limited at the macroscopic level, which also limits the achievable magnitude of strain gradients (i.e., <0.1 m^{-1}).[18] Notably, in earlier studies, even small macroscopic strain gradients could greatly enhance electric polarization in ceramic bulk solids.[44,45] However, the grain boundaries in these ceramics might contribute to the measured charge owing to their possible polar nature or surface piezoelectricity. Thus, it has long been difficult on the experimental side to realize purely flexoelectricity-related beneficial effects that are large enough to be considered for practical applications. It is also worth noting that the earlier studies on flexoelectric effects focus on ferroelectric oxides, wherein the flexoelectric response benefits from the high dielectric constants of the materials. There is growing interest in exploring giant flexoelectricity in other material systems such as polymers, semiconductors,[20] two-dimensional (2D) materials, halide perovskites,[21] and polar metals.[46]

Since the early 2010s, flexoelectricity has begun to reveal enormous scientific and technological potential in nanoscale materials (Fig. 1). Since the strain gradients are inversely proportional to the length scale, over which lattice deformation occurs, nanoscale materials could hold large strain gradients, and display considerable flexoelectric effects. This has motivated many studies to exploit flexoelectricity at the nanoscale, that is, what is called nanoscale flexoelectricity. For example, piezoelectricity turned out to be highly enhanced in nanostructured materials (e.g., a few hundred nanometers-thick, wavy piezoelectric ribbon) with strain gradients as large as 10^3 m^{-1}.[47] This observation corroborates the

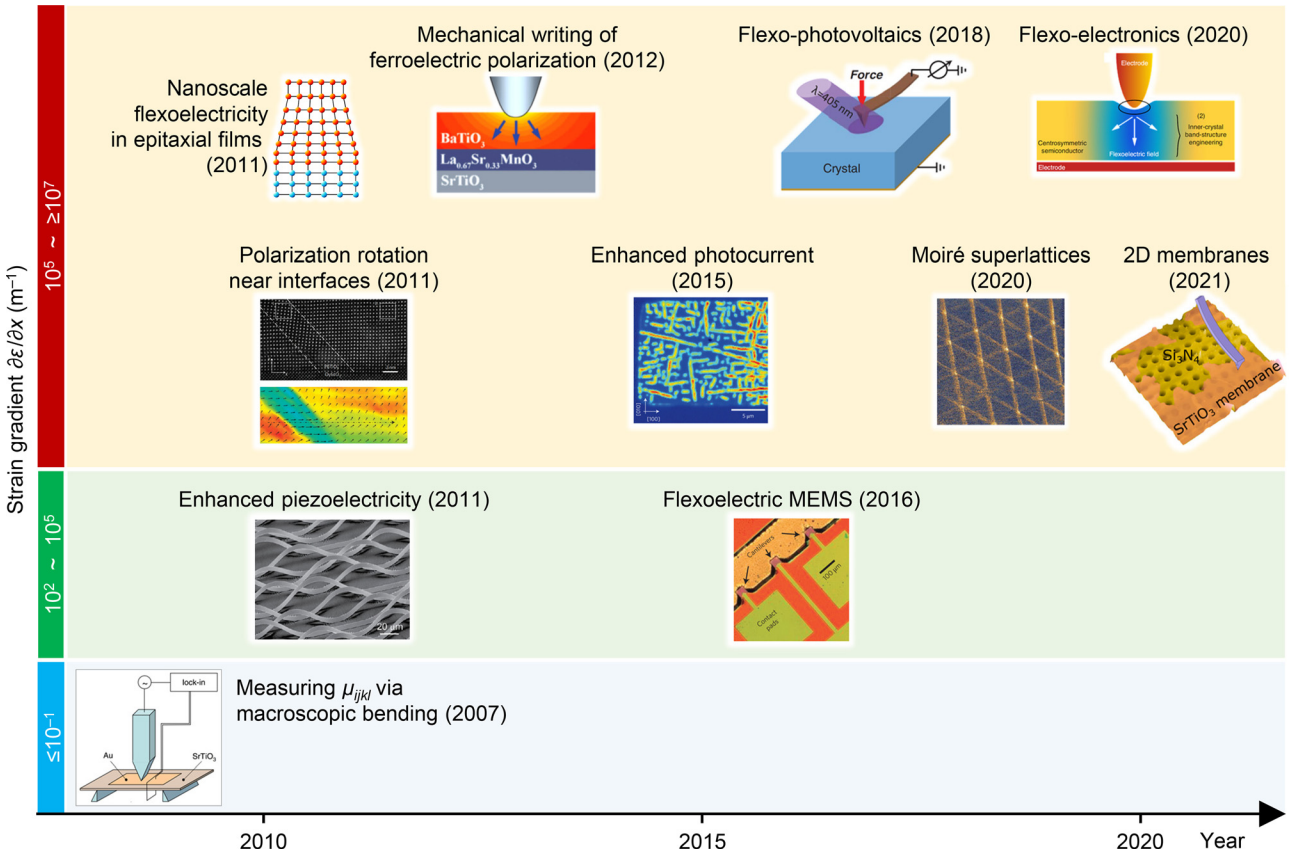

FIG. 1. Timeline of key milestones in the research of nanoscale flexoelectricity. In particular, the AFM tip pressing approach was developed in 2012 and has played a key role in the study of nanoscale flexoelectricity. Reproduced with permission from Zubko *et al.*, Phys. Rev. Lett. **99**, 167601 (2007). Copyright 2007 American Physical Society. Reproduced with permission from Qi *et al.*, Nano Lett. **11**, 1331–1336 (2011). Copyright 2011 American Chemical Society. Reproduced with permission from Lee *et al.*, Phys. Rev. Lett. **107**, 057602 (2011). Copyright 2011 American Physical Society. Reproduced with permission from Catalan *et al.*, Nat. Mater. **10**, 963–967 (2011). Copyright 2011 Springer Nature. Reproduced with permission from Lu *et al.*, Science **336**, 59–61 (2012). Copyright 2012 American Association for the Advancement of Science. Reproduced with permission from Chu *et al.*, Nat. Nanotechnol. **10**, 972–979 (2015). Copyright 2015 Springer Nature. Reproduced with permission from Bhaskar *et al.*, Nat. Nanotechnol. **11**, 263–266 (2016). Copyright 2016 Springer Nature. Reproduced with permission from Yang *et al.*, Science **360**, 904–907 (2018). Copyright 2018 American Association for the Advancement of Science. Reproduced with permission from Wang *et al.*, Nat. Nanotechnol. **15**, 661–667 (2020). Copyright 2020 Springer Nature. Reproduced with permission from McGilly *et al.*, Nat. Nanotechnol. **15**, 580–584 (2020). Copyright 2020 Springer Nature. Reproduced with permission from Harbola *et al.*, Nano Lett. **21**, 2470–2475 (2021). Copyright 2021 American Chemical Society.

previous theoretical study that predicted 400%–500% enhancement of the piezoelectric effect in nanoscale ferroelectrics[48] and underlines the technological potential of nanoscale flexoelectricity, especially in the design of micro- and nano-electromechanical systems. Interestingly, a thin-film cantilever actuator was later realized using only an active layer of $SrTiO_3$, which is originally non-piezoelectric, and its performance was comparable to that of state-of-the-art piezoelectric cantilevers.[15]

Using nanoscale materials with even larger strain gradients, Lee *et al.* also experimentally demonstrated the beneficial effect of nanoscale flexoelectricity in 2011.[19] Nanoscale epitaxial films could exhibit huge strain gradients,[49] due to the relaxation of misfit strains within the short length scale. For example, when the misfit strain of 1% relaxes through the thickness of 10 nm, the resulted strain gradient could be as large as $10^6\ m^{-1}$. This strain gradient is several orders of magnitude larger than those achievable by the mechanical bending of bulk solids and could result in electric polarization of around $10^{-2}\ C\,m^{-2}$. Therefore, the associated flexoelectric effect is sufficiently large to play an important role in, for example, controlling the ferroelectric domain configurations and polarization switching hysteresis loops.[19]

In the same year, an interesting study emerged,[50] which utilized intrinsic interfaces or boundaries within a material to achieve significant flexoelectric effects. Given the possibility of huge strain gradients occurring at the nanoscale, considerable flexoelectric responses could also arise near the structural inhomogeneities such as grain boundaries, phase boundaries, ferroelectric/ferroelastic domain boundaries, and dislocations.[50–56] Near those regions, flexoelectricity has been directly demonstrated by means of transmission electron microscopy. Catalan *et al.* observed the rotation of ferroelectric polarization at the *a*/*c* domain boundaries of $PbTiO_3$ epitaxial films near the interface with the substrate, using synchrotron x-ray diffraction and scanning transmission electron microscope imaging.[50] Although ferroelectric

materials usually possess the polarization in a specific crystal direction, the electric polarization vectors near *a*/*c* domain boundaries turned out to rotate continuously. Such a polarization rotation is closely related to enhanced piezoelectricity at the macroscale. This study therefore implies that nanoscale flexoelectricity could be useful for designing high-performance piezoelectric devices.

Despite some success in exploiting giant strain gradients in nanoscale materials, it has been challenging to dynamically and locally modulate the strain gradients. In this regard, it could be more effective to explore flexoelectricity by actively generating large strain gradients via external mechanical stress rather than simply using built-in strain gradients. In 2012, Lu *et al.* demonstrated that the flexoelectric effect induced by pure mechanical force from a sharp AFM tip could be used as a dynamic tool for ferroelectric polarization control.[57] This pioneering method, the so-called AFM tip pressing, has initiated extensive studies to manipulate various physical properties, ranging from ferroelectric domains,[57–64] oxygen vacancy concentration,[65–67] local transport behavior[22,68–70] to photovoltaic effect.[71,72] More details are covered later in Sec. V.

AFM has also been widely used for the detection of various functionalities near the region where huge strain gradients form. In 2015, Chu *et al.* discovered the anisotropic photocurrent behavior near the morphotropic phase boundary (MPB) of mixed-phase $BiFeO_3$ using angle-resolved photocurrent measurement.[73] The measured photocurrent turned out to be strongly linked to local strain gradients. Also, AFM has discovered intriguing local features near various regions where huge strain gradients develop, such as ferroelastic domain walls, mixed-phase boundaries, and wrinkled regions in 2D materials. Examples include the detection of topological polarization textures,[74] visualization of Moiré superlattices in two-dimensional materials,[75] and observation of local conduction in mixed-phase $BiFeO_3$ films.[72]

Very recently, there has been a growing amount of research related to flexoelectricity in 2D materials.[75–78] Since compared to typical bulk solids, 2D materials can show exceptional flexibility, a simple bending could result in huge strain gradients. Moreover, the recent development of exquisite methods for preparing various free-standing films[79,80] has widened the range of 2D materials. Indeed, it has been experimentally confirmed that those methods can be used to fabricate various 2D oxide membranes, even down to the monolayer limit. Therefore, 2D materials will serve as an interesting playground to explore emergent phenomena related to flexoelectricity.[81,82]

To summarize this section, nanoscale flexoelectricity has motivated extensive research over the past decade (Fig. 1), and its significance continues to grow with a broader scope of research. In particular, most of these studies are based on the AFM tip pressing technique. Therefore, it will be quite timely and important to establish a more solid basis for effective use of this technique. Sections III and IV will provide comprehensive guidelines for exploring nanoscale flexoelectricity via AFM tip pressing.

III. AFM TIP PRESSING AND RELEVANT EFFECTS

The AFM tip pressing onto a (polar) dielectric thin film is a complex process that can invoke the interplay of multiple physical and chemical effects coupled with the mechanical stimuli, aside from the flexoelectric effects. Some of these effects may compete with each other, bringing challenges to the interpretation of the AFM tip-induced phenomena. In this section, we discuss some of the other bulk effects that are inherent to the probed materials and can be mediated by the applied stress, as well as some surface effects associated with the AFM tip-film contact. Finally, we remark on possible strategies to distinguish the flexoelectric effect from the others.

A. Alternative mechanisms

1. Bulk electromechanical effects: Piezoelectricity, ferroelastic switching and structural phase transformation

The mechanical stress created by AFM tip pressing can modify the ferroelectric polarization via several electromechanical interactions. When the applied force is small, a linear and reversible piezoelectric response is expected. Usually, the polarization of a ferroelectric material varies in magnitude upon the applied pressure, or even rotates away from the polar axis under more complex loading conditions. After unloading, the pristine polarization state will recover. These reversible changes of polarization are accompanied by the modulation of local dielectric and piezoelectric responses, which could be probed *in situ* by using scanning probe techniques.

When the applied force increases, nonlinear electromechanical responses can be induced, such as ferroelastic switching and structural phase transformation. In multiaxial ferroelectrics, the tip pressing can induce non-180° polarization switching, such as the 90° ferroelastic switching from *c*-domain to *a*-domain in tetragonal $Pb(Zr,Ti)O_3$.[83] Such ferroelastic switching has recently been demonstrated to accommodate the AFM tip pressing-induced 180° reversal of polarization in 100-nm-thick $Pb(Zr,Ti)O_3$ films in which the tip-induced flexoelectric effect is limited.[84] In addition, the shear stress that can be significantly enhanced in the AFM tip scanning[64,85,86] has been shown to assist the ferroelastic switching and enable the reversal of the in-plane or out-of-plane polarization.[64,87,88] For example, the shear stress plays a governing role in the 71° ferroelectric domain switching in (001)-oriented rhombohedral $BiFeO_3$ films even without considering the flexoelectric effect.[64] A recent phase–field study also reveals the possibility of mechanically induced 180° polarization switching in ultrathin $BaTiO_3$ thin films by shear stress-mediated piezoelectric effects.[86] Accordingly, the shear stress-induced switching may overcome a known limitation of flexoelectricity-based mechanical writing, that is, the incapability of flipping the polarization from downward to upward due to the unidirectional nature of the AFM tip pressing-induced flexoelectric field.[57]

For ferroelectrics that can host coexisting polar phases at the nanoscale, such as the strain-stabilized morphotropic $BiFeO_3$ thin films,[89] the mechanical stimuli may induce structural phase transition accompanied by a modification of the polarization.[90,91] The mechanical formation of rhombohedral-like (R) nanophases within a tetragonal-like (T) phase matrix[91] by AFM tip pressing has been demonstrated in $BiFeO_3$ films grown on $LaAlO_3$ substrates. Reversibly switching between these R/T nanophases can be controlled by manipulating the tip scanning direction, resulting in the 180° rotation of the in-plane polarization[90] and tunability of the R/T phase population.[92] Both the ferroelectric switching and the structural transformation can give rise to piezoresponses in PFM, the interplay of which has recently been comprehensively investigated by Naden *et al.*[93]

2. Bulk mechanochemical effects: Vegard strain effect and chemical inhomogeneity

There also exist direct or indirect coupling effects between mechanical stress and the chemical concentration of point-defect species in the oxides, such as oxygen vacancies. One primary linear mechanochemical effect is the Vegard strain effect, which describes the lattice expansion due to accumulated chemical species, as well as the migration of the species under mechanical excitations. Usually, a linear dependence is assumed between the concentration of the species and the accompanying eigenstrains.[94] The Vegard effect is believed to determine the dynamics of oxygen vacancies under AFM tip pressing in oxide films, resulting in mechanical modulation of local electronic properties.[95,96] The mechanically induced migration of oxygen vacancies can also affect the polarization dynamics and may provide an alternative mechanism for the mechanical switching in relatively thick ferroelectric films.[97] AFM tip-induced reconfiguration of the oxygen vacancy distribution can also be achieved via a flexoelectricity-mediated mechanism, where the electrostatic depolarization field arising from tip-induced inhomogeneous polarization provides the driving force as suggested in non-ferroelectric $SrTiO_3$ thin films.[67]

The preexisting chemical inhomogeneities in the probed material can also give rise to flexoelectric-like responses to the applied nonuniform deformation.[98–100] The alignment of dipolar defects in complex oxides and non-stoichiometric systems is believed to be responsible for the macroscopic symmetry breaking in otherwise centrosymmetric ceramics and single crystals.[100–103] Built-in composition gradients by design can create polarity in otherwise nonpolar systems[104] and enhance domain wall mobility for electromechanical responses.[105] Moreover, a recent design shows markedly enhanced and tunable flexoelectricity upon bending by implanting net charges into a bimorph structure made of polar soft materials, opening the concept of flexoelectrets.[106] However, although the coupling between chemical inhomogeneities and mechanical stress has been extensively studied macroscopically, less is known about the counterpart mechanochemical interaction at the nanoscale, awaiting further exploration by using AFM tip pressing.

3. Surface effects: Surface electrochemistry, surface piezoelectricity, and triboelectric effect

Surface effects due to the interaction between an AFM tip and the polar surface of the probed material are also important for a comprehensive understanding of the process of tip pressing.[107] The polar surface of a ferroelectric thin film is usually screened by charged adsorbates from the ambient environment, such as hydrogen and hydroxyl species. The removal or segregation of these mobile species can remarkably change the electric boundary condition on the surface and influence the stability of ferroelectric polarization.[103] For example, 180° polarization switching can be induced in ultrathin $PbTiO_3$ films by properly controlling the partial pressure of oxygen of the ambient, which is known as chemical switching.[108] The application of a mechanical force can be regarded as imposing an effective electric field that shifts the electrochemical potential of the chemical species, whether it is charged or neutral, and thus modulates its concentration in the proximity of the contact region. Cao *et al.*[97] has given a quantitative analysis of the surface electrochemical process based on a phase–field model incorporating the ferroelectric ordering and surface electrochemistry.[109] Notably, the mechanical pressure can shift the electrochemical potential in a highly nonlinear way, depending on the type of species and the magnitude of the applied force.

Other possible modifications to the surface boundary condition, such as by the bulk flexoelectric effect[110] or surface piezoelectricity,[111] have also been suggested. As theoretically shown by Chen *et al.*,[112] a ripple-like domain pattern and the possibility for downward-to-upward polarization switching can be realized by manipulating the extent of surface screening. Moreover, the symmetry-breaking nature of a free surface can bring polarity to the otherwise nonpolar bulk materials. Recent experiments reveal appreciable surface pyroelectricity[113] and surface polarization[114] on the (001)-surface of cubic $SrTiO_3$, which is macroscopically nonpolar. In this sense, electromechanical coupling effects such as surface piezoelectricity are expected to be displayed in $SrTiO_3$ and similar systems under mechanical loading, whereas such an attempt has not yet been made.

A recent discussion on the role of flexoelectricity in triboelectricity brings a new ingredient to the long-standing issue of the origin of triboelectricity.[115,116] It is believed that the charge transfer originates from a flexoelectricity-induced electrical potential during indentation and pull-off of the two contacts at the nanoscale. In this sense, we may also expect that the AFM tip scrapping on the sample surface not only modifies the distribution of original screening species but also "injects" charges into the film. This conjecture is evidenced by Kelvin probe force microscopy (KPFM)-based experimental measurements that show that the tip rubbing changes the surface potential of a ferroelectric co-polymer film differently depending on the pre-poled direction.[117] Another study on the tribological properties of ferroelectric materials reports a lubrication effect on the dry friction by up to 40% with the application of tip stress on the (001) surface of $BiFeO_3$.[118] In addition, the thermal effect associated with tip rubbing may also affect the stability of ferroelectric polarization.[119] Therefore, more crossover between flexoelectricity and tribology is anticipated to advance the fundamental understanding and application of both fields.

Notably, many experiments have demonstrated mechanical switching capabilities in thick films (of several hundreds of nanometers)[120–122] or in systems where the domain structures and polarization configurations are complex, such as in polycrystalline films,[120–123] relaxor-ferroelectric crystals,[124,125] $Pb(Zr,Ti)O_3$ near the MPB,[126] superlattices with polar vortex arrays,[127,128] and flexible oxide membranes.[81,129] Complicated by the microstructural features and polar heterogeneity in these systems, some of the above-mentioned effects and other secondary effects involving the dynamics of multiple domains may play synergistic roles.[86] For example, it has recently been demonstrated that the 180° ferroelectric switching can be achieved by a ferroelastic domain-mediated process in 100 nm-thick $Pb(Zr,Ti)O_3$ films where the flexoelectric contribution is marginal.[84]

B. Possible strategies for distinguishing the flexoelectric effect from the others

After displaying several primary effects relevant to the AFM tip pressing, we turn to discuss possible strategies to identifying the role of flexoelectricity among other effects. In principle, this can be demonstrated by properly excluding other factors through minimizing their contributions or by directly establishing a connection between the

measured quantities and the applied stress gradient. The latter strategy requires an accurate assessment of the stress gradient, which will be discussed in Sec. IV B.

1. Minimizing artifacts

Unwanted artifacts relevant to the characterization of SPM techniques should be excluded. For example, the electrostatic interaction between the tip and the sample may be ruled out by reproducing the AFM tip force-induced effects with a tip coated by nonconductive materials.[57,64,67] It can also be minimized by using the cantilevers with relatively high spring constants.[130] However, one should carefully consider that such stiff cantilevers would also give less sensitivity in the measurements of ferroelectric domains. The applied mechanical force should not exceed the critical value for plastic deformation of the sample, which may cause damage visible in the topographic image of the surface.[131]

It might be possible to exclude the involvement of an electrochemical process by showing that the observed phenomena are reproducible by repeated exertion/withdrawal of the loading force. The use of a graphene top electrode could furthermore make it possible to exclude the electrochemical interaction of a probed material with the AFM tip or ambient atmosphere,[69] as graphene is impermeable to all atoms and molecules.

2. Scan rate-dependent experiments

The establishment of chemical equilibria of ionic species in solids is generally much slower than that of the relaxation of lattice deformation or polarization at room temperature.[132] Therefore, scanning rate-dependent measurements can be utilized to rule out the bulk or surface electrochemistry effects.[67] Here, we provide one example to illustrate how to determine the characteristic timescales of relevant kinetic processes and design proper scanning-rate experiments to figure out the primary mechanism for the tip-induced polarization switching. The AFM tip pressing-induced polarization switching in ferroelectric ultrathin films can be ascribed to the flexoelectric effect or the bulk migration of oxygen vacancies.[97] The flexoelectric mechanism has been shown to occur at a timescale similar to that of the bias-induced local polarization switching,[133] which is governed by the sideway motion of domain walls. It has been shown that the domain wall velocity v_{DW} obeys the creep kinetics in the intermediate electric field regime,[134] which can be written as

$$v_{DW} \sim \exp\left[-\frac{U}{k_B T}\left(\frac{E_{C0}}{E}\right)^{\mu}\right], \tag{2}$$

where E is the applied electric field, T is the temperature, and k_B is the Boltzmann constant. The energy barrier U, threshold depinning field E_{C0}, and the critical exponent μ can be determined from experimental measurements[134] or atomistic simulations.[135] Given that the local effective flexoelectric field can reach as high as 100 MV m^{-1}, we can estimate the domain wall velocity to be $v_{DW} \sim 0.05$ m s^{-1} in $PbZr_{0.2}Ti_{0.8}O_3$ epitaxial thin films at room temperature according to Ref. 134. In this sense, a typical timescale for the domain wall to propagate across a length scale $L \sim 100$ nm is calculated as $\tau_{DW} \sim 2$ μs.

In contrast, the oxygen vacancy-mediated mechanism exhibits much slower kinetics at room temperature, which can be estimated as follows by calculating the mobility μ_m of the charged species. The mobility μ_m of the oxygen vacancy $V_{\ddot{O}}$ can be estimated by using the Nernst–Einstein relation and the Arrhenius law for the temperature dependence of the diffusivity,[136] that is,

$$\mu_m = \frac{\mu_0}{T}\exp\left(-\frac{E_a}{k_B T}\right), \tag{3}$$

where μ_0 is the prefactor, and E_a is the activation energy. The latter two parameters can be determined from experiments or calculated by atomistic simulations.[137] For typical perovskite oxides such as $BaTiO_3$, the mobility of $V_{\ddot{O}}$ at room temperature is estimated to be $\mu_m \sim 10^{-12}$ cm^2 V^{-1} s^{-1}.[138] Assuming the same effective electric field of $E \sim 100$ MV m^{-1}, the drift velocity of $V_{\ddot{O}}$ is $v_{V_{\ddot{O}}} = \mu_m E = 10$ nm s^{-1}. Therefore, the typical timescale for $V_{\ddot{O}}$ to drift across the same length scale $L = \sim 100$ nm is $\tau_{V_{\ddot{O}}} \sim 10$ s. Note that $\tau_{V_{\ddot{O}}}$ is larger than τ_{DW} by several orders of magnitude.

The huge difference in the kinetics of the two mechanisms allows one to design scanning rate-dependent experiments to differentiate the primary mechanism for the tip-induced polarization switching. For example, one can perform a series of tip scanning experiments with a fixed above-threshold loading force to generate an equivalent flexoelectric field ~100 MV m^{-1} and with an increasing scanning rate (the typical range of scanning rate can be $v_{tip} = 0.1$–10 μm s^{-1}) to suppress the impact of the contribution from the bulk migration mechanism. In this sense, the competing mechanism aside from the flexoelectricity for the polarization switching can be gradually eliminated.

From the example above, one can see that a careful estimation of the timescale of the primary kinetic processes is critical for distinguishing the flexoelectric mechanism among others. Other approaches to reduce the influence of surface electrochemistry include examining the reversibility of the tip pressing-induced effect,[64,68,69] or reproducing the phenomena in ultrahigh vacuum environment.[95]

3. Ruling out other electromechanical responses

Under AFM tip pressing, large strains and strain gradients inevitably coexist, bringing challenges to separating the effects from strains and strain gradients in experiments. One possible approach is to modulate the flexoelectric contribution by systematically controlling strain gradients via several AFM tips with varied tip radii (Fig. 2), as demonstrated in Refs. 67 and 69. Importantly, increasing the radius of the AFM tip could suppress the induced strain gradient to a greater extent than the strain. Therefore, whether the strain or the strain gradient is governing in the process can be determined. Figure 2(c) shows the case when plotting the data as a function of strain gradients, all of the data obtained with different AFM tips collapses to a nearly single curve. In such a case, the close correlation between the experimental observation and the strain gradients could be emphasized, which signals the dominant role of flexoelectricity among other mechanisms.

In addition, theoretical analysis and numerical modeling have often been complemented to single out the most relevant effect from the various electromechanical and mechanochemical coupling effects.[86,97,139–141] Admittedly, it is highly desirable to develop a comprehensive model that self-consistently incorporates the statics and dynamics of several order parameters, as well as the transport

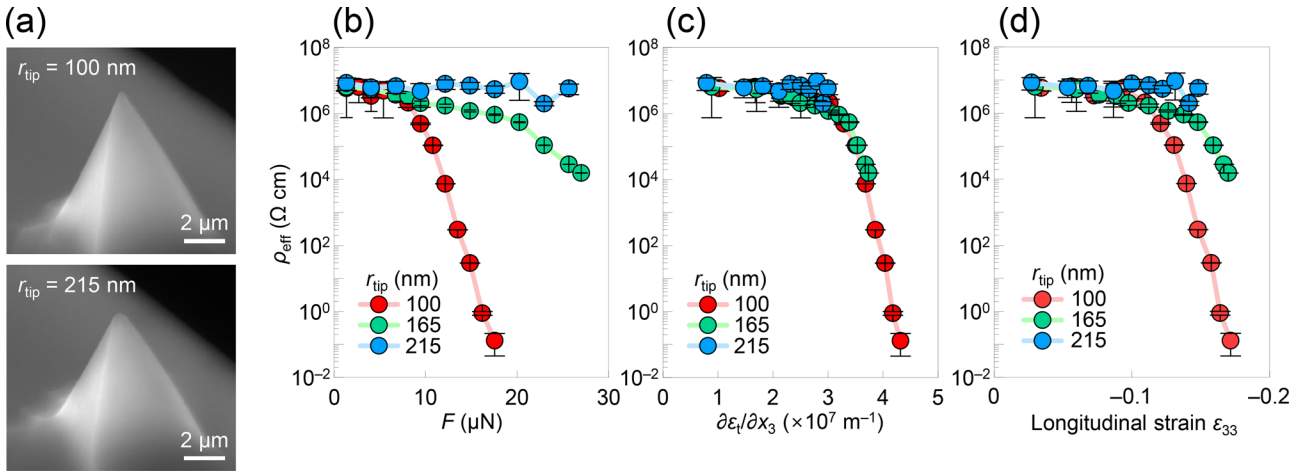

FIG. 2. How to directly show the close correlation between the experimental observation and strain gradients. (a) Scanning electron microscopy images of the AFM tips with different tip radii (r_{tip}). (b) Experimental data (i.e., electrical resistivity ρ_{eff}) measured as a function of tip loading force F. (c) ρ_{eff} plotted as a function of the AFM tip-induced strain gradient $\partial\varepsilon_t/\partial x_3$. (d) ρ_{eff} plotted as a function of the AFM tip-induced longitudinal strain ε_{33}. Reproduced with permission from Park *et al.*, Nat. Commun. **11**, 2586 (2020). Copyright 2020 Author(s), licensed under a Creative Commons Attribution 4.0 License.

behaviors of chemical species, to provide better understanding of the AFM tip pressing-induced phenomena. A detailed review of recent progress toward this direction is given in Sec. IV B 5.

To conclude this section, Table I summarizes some of the mechanisms mentioned above and possible experimental or theoretical approaches to separate their contributions.

IV. BASIC CHARACTERIZATION METHOD

A. Estimation of the applied force by AFM tip

To properly assess the flexoelectricity contribution to the AFM tip pressing-induced phenomena, it is critical to accurately evaluate the magnitude of the applied stress/strain gradient. This indicates that

TABLE I. Possible AFM tip pressing-induced effects and strategies to identify their contributions.

AFM tip pressing-induced effects	Description	Possible strategies to identify	Reference
Bulk electromechanical coupling effects			
Flexoelectric effect	Stress-induced flexoelectric field for polarization switching	Numerical simulations with on/off flexoelectricity; Expected to be unidirectional switching	64, 139, 141
Ferroelastic switching	Stress-induced ferroelastic switching and associated polarization switching	Expected to be bidirectional switching; May occur even in thick films	
Structural phase transition	Stress-induced structural phase transition and associated polarization switching	Expected to be independent of polarization direction; Significant changes in surface topography	90, 91
Bulk mechanochemical coupling effects			
Vegard strain effect/chemical pressure	Stress-induced redistribution of point and dipolar defects	Scanning rate-dependent measurement; Repeated experiments	67, 132
Surface effects from the interaction between the tip and film			
Electrostatic effect	Long-range Coulomb effect between tip/cantilever and film	Use grounded or insulator coated AFM tip; Use stiffer cantilevers	107
Surface electrochemistry	Mechanically erasing/accumulating adsorbates that modify the surface screening	Ultrahigh vacuum experiments; Scanning rate-dependent measurement	97
Triboelectricity	Charge transfer due to contact, scanning, and pull-off	Measuring surface potential before and after loading	117

it is first required to estimate the applied force by AFM tip. The contact force F between the tip and the sample can be calculated using Hooke's law, that is, $F = k \times d$, where k and d are the spring constant (N/m) and the deflection (m) of the AFM cantilever, respectively. The cantilever with a nanosized sharp tip at its end is the central part of laser beam deflection-based AFMs. Interactions between the tip and the sample lead to the deflection of the cantilever d. The d value can be measured by a laser beam-based simple optic system. A focused laser beam is directed onto the top side of the cantilever, and the reflected beam hits a four-segmented position-sensitive photodetector (PSPD). Consequently, PSPD measures the vertical and lateral movements of the laser beam, which correspond to the vertical and lateral deflection of the cantilever. Since the PSPD provides the signals with voltage unit (V), the conversion factor between the PSPD signal and the cantilever deflection [i.e., the so-called inverse optical lever sensitivity, InvOLS (m/V)] should be needed to calibrate d. The measurement of the force–distance curve is a well-known and simple method to estimate the InvOLS value for vertical deflection.[142,143] This method measures the voltage signal of PSPD as a function of the known distance moved by the piezo (equivalent to d) when the tip is pushed into the sample surface. The PSPD voltage–distance curve is a linear line in the tip-surface contact region, and thus, the InvOLS value can be obtained from the slope of this curve. For the determination of the spring constant k, there exist several techniques, including the Cleveland method[144] and Sader method.[145] The Cleveland method is to calculate k by measuring the change in the cantilever's resonance frequency before and after attaching a known mass to the end of the cantilever. The Sader method is to determine the k value of a rectangular cantilever by measuring the resonance frequency and quality factor of the cantilever in fluid (typically, air). Here, we introduce another typical method, the thermal noise method, which measures the thermal noise of the cantilever based on the equipartition theorem,[146] since many commercial AFM machines provide it as a basic function, so it is now widely used. For small deflections, an AFM cantilever can be approximated as a simple harmonic oscillator with one degree of freedom. By measuring the power spectral density of the thermal fluctuations in tip displacement in the frequency domain, the k value can be estimated by $k = k_B T/P$, where P is the area of the power spectrum of the thermal fluctuations alone. Two of the most widely used methods, the Sader method and the thermal noise method, have fundamentally different advantages and disadvantages.[147] The Sader method is not very sensitive to an error affecting the scale of AFM deflection measurements, unlike the thermal noise method. However, the Sader method is designed only for low fluid loading conditions, while the thermal noise method is effective regardless of the amount of fluid loading. The relative uncertainties of these methods for the spring-constant calibration typically range from 10% to 30%.[148,149] In conclusion, the vertical contact force by AFM tip can be calibrated as follows: $F = k \times \text{InvOLS} \times \Delta\text{PSPD}$, where ΔPSPD (V) is the vertical change of the PSPD signal.

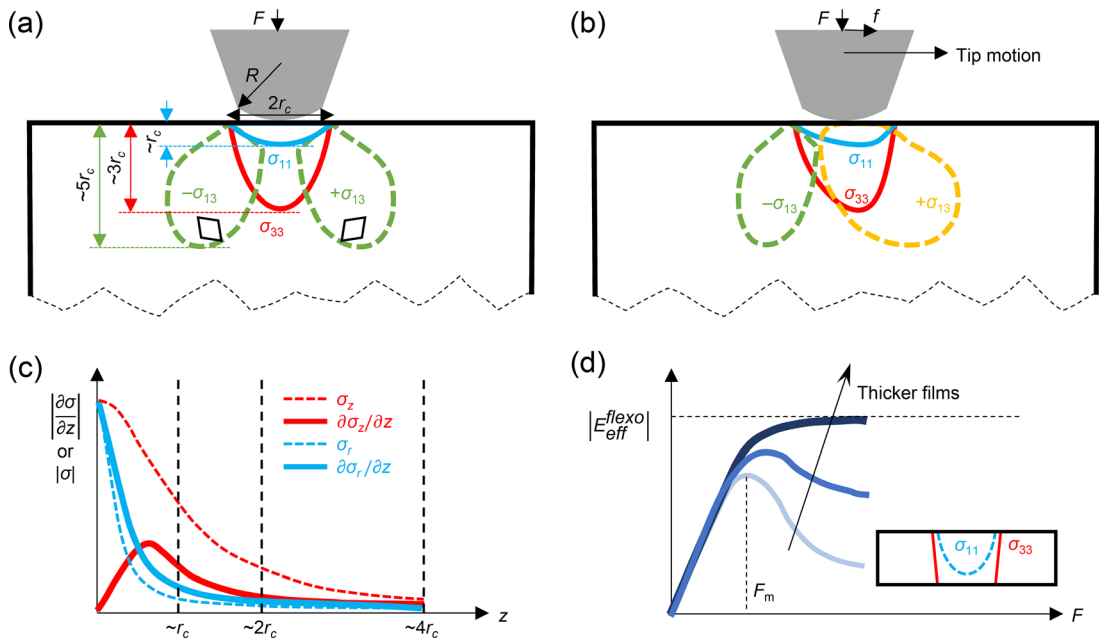

FIG. 3. Schematics of typical features for the stress gradients induced by AFM tip pressing. (a) Spatial distribution of longitudinal stress σ_{33} (red solid curves), transverse stress σ_{11} (blue dotted curves), and shear stress $\pm\,\sigma_{13}$ (green dashed curves) under AFM tip pressing with a loading force F. The tip is modeled as a spherical indenter with radius R that generates a circular contact area with a radius r_c. The contours show the locus where the corresponding stress component reduces to ~1/10 of the maximal value. For shear stress, there are two lobes for positive or negative shear stresses, as indicated by the rhombus symbol. (b) Spatial distribution of the same stress components under a scanning AFM tip with a loading force F and a tangential frictional force f. The symbols are consistent with (a). The two lobes of the shear stress $\pm\,\sigma_{13}$ become asymmetric due to the tangential force while the distributions for the other stress components are also affected. (c) The profiles of normalized longitudinal stress σ_z, lateral stress σ_r, and their gradients along the out-of-plane direction ($\partial\sigma_z/\partial z$ and $\partial\sigma_r/\partial z$) from the contact center into the film. (d) The magnitude of the effective flexoelectric field E_{eff}^{flexo} as a function of the loading force F (for the normal loading) in films of various thicknesses. F_m indicates the force corresponding to the maximal E_{eff}^{flexo}. The inset shows the nearly-homogenous stress distributions in an ultrathin film under a high loading force wherein E_{eff}^{flexo} is largely reduced.

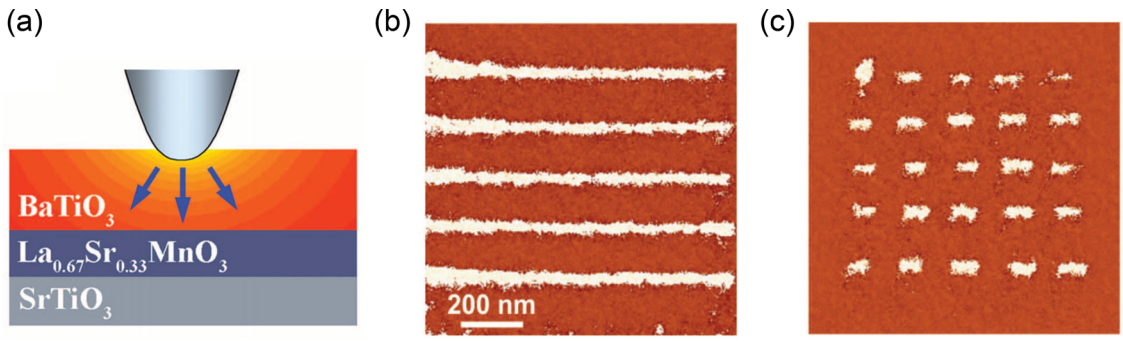

FIG. 4. Flexoelectric switching of ferroelectric polarization via AFM tip pressing. (a) Schematic illustrating the strain gradient and associated flexoelectric field induced by the AFM tip pressing the surface of ultrathin $BaTiO_3$ films. PFM phase images of domain (b) lines and (c) nanodots mechanically written in the ultrathin $BaTiO_3$. Reproduced with permission from Lu *et al.*, Science **336**, 59–61 (2012). Copyright 2012 American Association for the Advancement of Science.

B. How to estimate strain/stress gradients

Although some experimental methods to measure strain gradients exist,[50,150] direct measurements of AFM tip-induced strain gradients are still challenging experimentally. Therefore, to estimate the strain gradients, it is often necessary to obtain the strain distribution under the tip contact by theoretical approaches, including analytical calculations and numerical simulations. In the following, we briefly review the theoretical methods for estimating the strain/stress gradients in the tip pressing scheme.

Unlike the commonly used methods for measuring flexoelectricity macroscopically, such as the cantilever bending or pyramid compressing,[30] the AFM tip pressing at the nanoscale has a complicated geometry and may thus introduce multiple strain gradients. The classical Hertzian theory of contact mechanics, though originally developed for non-adhesive elastic indentation of a semi-space, has often been adopted as a first approximation.[151] In the framework of the Hertzian contact mechanics, the sharp AFM tip can be modeled as a spherical indenter with a tip radius R, which is usually around a few tens of nanometers. The film–substrate heterostructure can be treated as a semi-infinite space if its thickness t is much larger than the contact radius r_c (i.e., the radius of the circle of contact, typically around 10 nm under $\sim$1.0 μN load). When isotropic elasticity is assumed, the contact radius can be expressed as

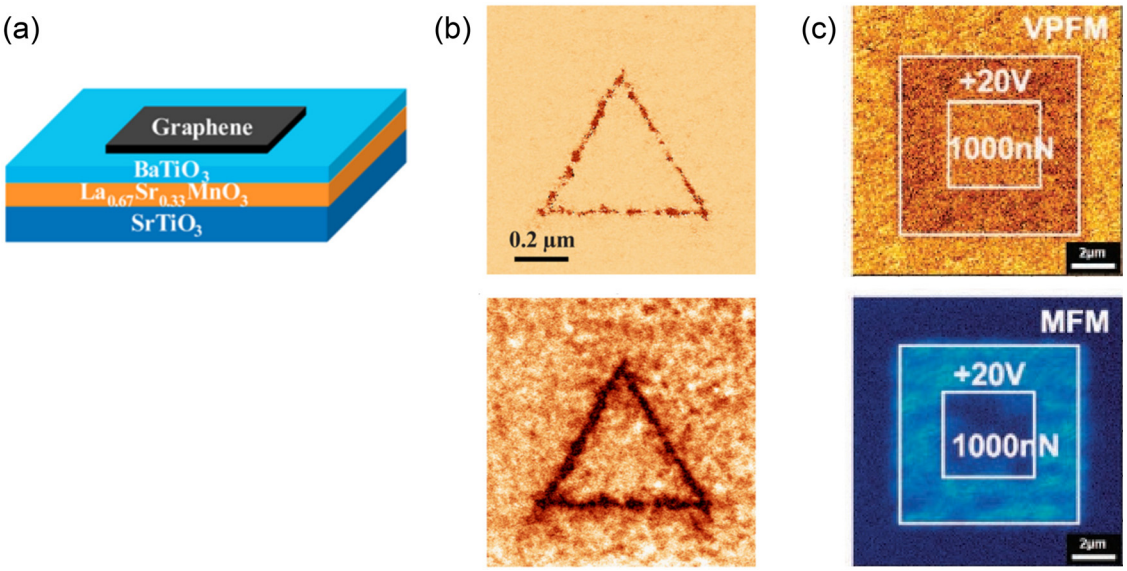

FIG. 5. Flexoelectric switching of polarization in various ferroelectric systems. (a) Schematic of the ferroelectric $BaTiO_3$ with graphene electrode. (b) Out-of-plane PFM phase (top) and amplitude (bottom) images with mechanically written domain lines in the ultrathin $BaTiO_3$ film in (a). Reproduced with permission from Lu *et al.*, Nano Lett. **16**, 6460–6466 (2016). Copyright 2016 American Chemical Society. (c) Out-of-plane PFM phase (top) and MFM phase (bottom) images with the mechanically written region in multiferroic $Bi_5Ti_3FeO_{15}$ film. Reproduced with permission from Jia *et al.*, NPG Asia Mater. **9**, e349 (2017). Copyright 2017 Author(s), licensed under a Creative Commons Attribution 4.0 License.

$$r_c = \left(\frac{3}{4}\frac{FR}{E^*}\right)^{1/3}, \tag{4}$$

where F is the contact force by the AFM tip (as described in Sec. IV A), and E^* is the effective modulus of the contact, that is, defined by the elastic moduli E and Poisson's ratios ν of the tip and the film, that is,

$$\frac{1}{E^*} = \frac{1-\nu_{\text{tip}}{}^2}{E_{\text{tip}}} + \frac{1-\nu_{\text{film}}{}^2}{E_{\text{film}}}. \tag{5}$$

Then, the normal stress distribution on the surface within the contact area can be formulated as

$$\sigma_z(r) = -\frac{3}{2}\left(\frac{F}{\pi r_c{}^2}\right)\left(1-\frac{r^2}{r_c{}^2}\right)^{1/2}, \tag{6}$$

where $r\ (\leq r_c)$ measures the distance from the contact center. The full analytical expressions of the mechanical displacement and other strain and stress distributions interior of the indented specimen for isotropic media can be found in textbooks of contact mechanics.[151] A simple estimation of the strain and stress gradients can be made by simple algebraic calculations therein. Despite its simplicity and origins for describing macroscopic phenomena, the Hertzian contact mechanics have been widely utilized to gain some insights into the AFM tip pressing-induced phenomena at the nanoscale.[71,115]

Here, we provide some simple analysis based on the Hertzian theory to illustrate some key features of the AFM tip pressing-induced stress/strain gradients in the probed film. Figure 3(a) schematically shows the spatial distributions of the longitudinal, transverse, and shear stress components interior of the half-space beneath the contact region of a spherical indenter. The contours correspond to the loci at which the magnitude of the stress component is reduced to approximately 10% of its maximal value. It is evident that the longitudinal stress σ_z (solid red) has a relatively deeper penetration depth than that of the transverse stress σ_r (blue dotted), resulting in smaller $\partial\sigma_z/\partial z$ than $\partial\sigma_r/\partial z$ near the surface [Fig. 3(c)]. The shear stress component has the deepest penetration while splitting into two symmetric lobes with opposite directions (green dashed).

When the tip is scanning across the surface, a tangential frictional force may be imposed onto the film surface. As a first approximation, the frictional force yields shear stress along the surface, that is, proportional to the normal stress, that is, $\sigma_{zr}(r) = k_f\,\sigma_{zz}(r)$, where k_f denotes the friction coefficient. Under this circumstance, the corresponding stress distribution in the film is distorted and becomes asymmetric, as schematized in Fig. 3(b). In particular, the shear stress, that is, in front of the AFM tip motion direction (orange dashed) is significantly enhanced in magnitude and affected area, while the other lobe of the shear stress behind the tip motion is reduced in size. This friction-induced modulation of the stress and stress gradients is associated with strong in-plane flexoelectric fields that depend on the scanning direction of the AFM tip and thus enables selective control of ferroelectric domain switching in multiaxial ferroelectrics such as $BiFeO_3$ thin films.[64]

We further qualitatively estimate the vertical gradients of these stress components and examine their dependences on the loading force and film thickness. This analysis leads to some nontrivial results, as illustrated in Figs. 3(c) and 3(d). For example, the out-of-plane gradient of the transverse stress, $\partial\sigma_r/\partial z$, decays quickly from the film surface with a characteristic depth of $\sim r_c$ (solid blue curve). In contrast, the out-of-plane gradient of the longitudinal stress, $\partial\sigma_z/\partial z$, is almost zero at the surface, but peaks at a depth below r_c before decaying. We also notice that the normalized flexoelectric field E_{eff}^{flexo} [calculated by taking the value of the flexoelectric coefficients of $BaTiO_3$ (Ref. 141)] exhibits nontrivial dependence on the applied normal force F for different film thicknesses [Fig. 3(d)]. For relatively thick films, E_{eff}^{flexo} increases linearly with F and then saturates, while for ultrathin films, E_{eff}^{flexo} saturates at a smaller force and then decays as F increases further. In other words, the applied loading force F_m for maximized flexoelectric field increases with the film thickness. The lowering of E_{eff}^{flexo} in ultrathin films at relatively larger F can be understood by the fact that the spatial region affected by the tip pressing continues to widen and penetrate across the entire film thickness, thus lowering the effective strain gradient within the region as F increases further. The distinctive force-dependent behavior for ultrathin and relatively thick films can help to rationalize the counterintuitive thickness dependence of the mechanical switching behavior in

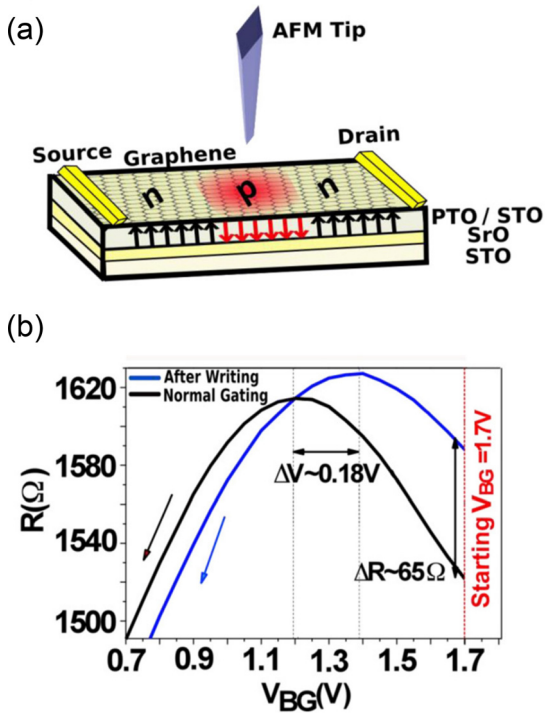

FIG. 6. Mechanical gating via AFM tip pressing. (a) Schematic depicting that the mechanically down-poled region is p-doped. The exfoliated graphene was deposited on a 100-nm-thick $PbTiO_3/SrTiO_3$ (PTO/STO) ferroelectric superlattice to fabricate a graphene-ferroelectric-field-effect-transistor (GFeFET) device. Mechanical writing with an AFM tip is an effective way to locally create a "down-polarization" domain beneath the graphene in the PTO/STO superlattice, and negative bound charges at the interface between graphene and superlattice lead to hole doping in the graphene. (b) Graphene transport properties show hole doping after writing. The local down-polarization domains populate the graphene with holes, as evidenced by the positive gate voltage shift of $\Delta V = 0.18$ V in the resistance maximum. Reproduced with permission from Yusuf *et al.*, 2D Mater. **4**, 021022 (2017). Copyright 2017 IOP Publishing.

$BaTiO_3$ thin films.[141] Moreover, this result also suggests that enlarging the loading force may not always facilitate flexoelectricity-enabled mechanical switching of ferroelectric polarization.

It should be noted that the classical Hertzian theory is based on several assumptions that may not properly apply to the AFM tip pressing of thin films of a few nanometers thickness. Many contact mechanics models have been developed based on the Hertzian theory to account for the piezoelectric coupling[152–156] and the finite thickness effect.[157–160] Several considerations need to be made before choosing an appropriate contact mechanics model. Here, we highlight a few critical ones and summarize recent advances in the contact mechanics theory that can offer more accurate evaluation of the strain/stress gradients for the AFM tip pressing at the nanoscale.

1. Transverse anisotropy of the material

The closed-form analytical solution of the electro-elastic fields for a transversely isotropic piezoelectric half-space under an elliptic indenter has been derived.[152,153,155,161–164] Notably, these solutions are derived based on the axisymmetric assumption, which can serve as a valid approximation for systems such as pre-poled piezoceramics. For single-crystalline ferroelectric films with strong in-plane polarization anisotropy, for example, when the polarization is not perpendicular to the film surface, such an analytical solution may not be valid. Although a generalized closed-form formulation of the stress fields under indentation considering full anisotropy of piezoelectricity has been given by using Stroh's formalism and Fourier transform techniques,[165] it usually requires numerical solving of a set of integral equations.

2. Finite thickness of the film and elastic properties of the substrate

This consideration is of particular importance when the film thickness is comparable to the contact radius or when the substrate material has distinct elastic or piezoelectric properties. In this sense, the film may be considered as a thin coating layer on a thick substrate that can be treated as a semi-infinite space. For a piezoelectric active thin layer, Wang *et al.* developed the generalized solution for the electro-elastic fields within the film on a rigid substrate.[158] The theory has then been extended to situations wherein the substrate is compliant or is perfectly bonded with the film allowing for the transfer of deformation.[159,166,167] Note that closed-form solutions are available only for the ultrathin and ultrathick limits, while for the intermediate cases, numerical results are, in general, sought. Very recently, the effect of substrate elasticity on the AFM tip-induced ferroelectric switching has been studied using phase–field modeling.[168]

3. Treatment of the friction force

Although in the analysis above, the friction is modeled as the tangential surface traction proportional to the normal traction, a rigorous treatment needs to account for the change in shape of the contact area, which may become non-axisymmetric. The finite element simulations[85,86] show that the contact area and the associated strain/stress field are significantly changed due to the tip motion. Recent analytical theory[169–171] and finite-element simulations[172] have considered the fractional sliding effect for a piezoelectric half-space[171] or thin films,[119,173] wherein the frictional heat generation has also been considered.[119]

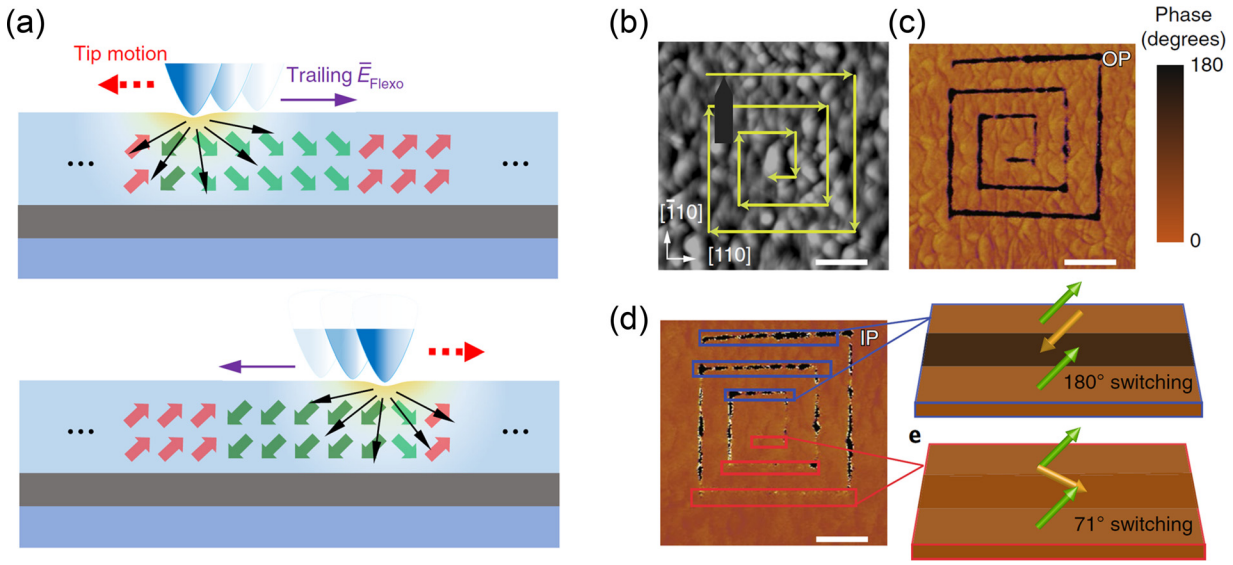

FIG. 7. Flexoelectric switching of multiaxial ferroelectric polarization. (a) Schematics of the trailing flexoelectric field ($\bar{E}_{Flexo}$) and corresponding polarization switching in a $BiFeO_3$ film tracing the tip motion. (b) Schematic of the mechanical line scan pattern overlaid on a topography image of the scanned region. Yellow arrows indicate the direction of tip movement. The black arrow represents the shape of the SPM tip indicating the IP sensitive direction of PFM measurement. The (c) out-of-plane and (d) in-plane PFM phase images after mechanical scanning on a $BiFeO_3$ thin film. The scale bars represent 600 nm. Reproduced with permission from Park *et al.*, Nat. Nanotechnol. **13**, 366–370 (2018). Copyright 2018 Springer Nature.

4. AFM tip-induced evolution of the microstructure

When the AFM tip pressing changes the microstructure of the film (e.g., mechanical switching of the ferroelectric/ferroelastic domains), the contact mechanics problem needs to be coupled with the evolution of the microstructure in the material, which can be conveniently described by the phase–field method.[174] For example, in ferroelectric materials, the Landau–Ginzburg–Devonshire (LGD) theory of ferroelectrics has been exploited to study the nucleation and switching of domains under applied electromechanical fields by the AFM tip.[140,175] The coupling between the order parameters (e.g., the ferroelectric polarization) and the mechanical strains can be treated by Khachaturyan's microelasticity theory[176] for fully anisotropic and structurally inhomogeneous systems subject to various electromechanical boundary conditions,[177,178] including the AFM tip pressing.[112,139] The surface traction due to AFM tip pressing and scanning enters the elastic equilibrium equation in the phase–field model as a boundary condition at the film surface, which may be approximated by using an appropriate analytical solution from the Hertzian-like models[139] or by numerical computation via finite-element modeling.[112] Recent advances in the phase–field model have successfully incorporated the vibrational dynamics of polarization,[179] which allows for exploring the electromechanical responses under ultrafast stimuli.[180]

5. More accurate estimation of the strain/stress gradients

Several advances have been made recently in the contact mechanics theory of piezoelectrics, which can be further implemented for numerical evaluation of the strain gradients under AFM tip pressing. For example, surface effects such as residual surface stress and surface piezoelectricity have been considered for a piezoelectric half-space.[181] The impact of such surface effects on the tip pressing-induced domain switching has been studied.[182] The adhesion effect has been examined

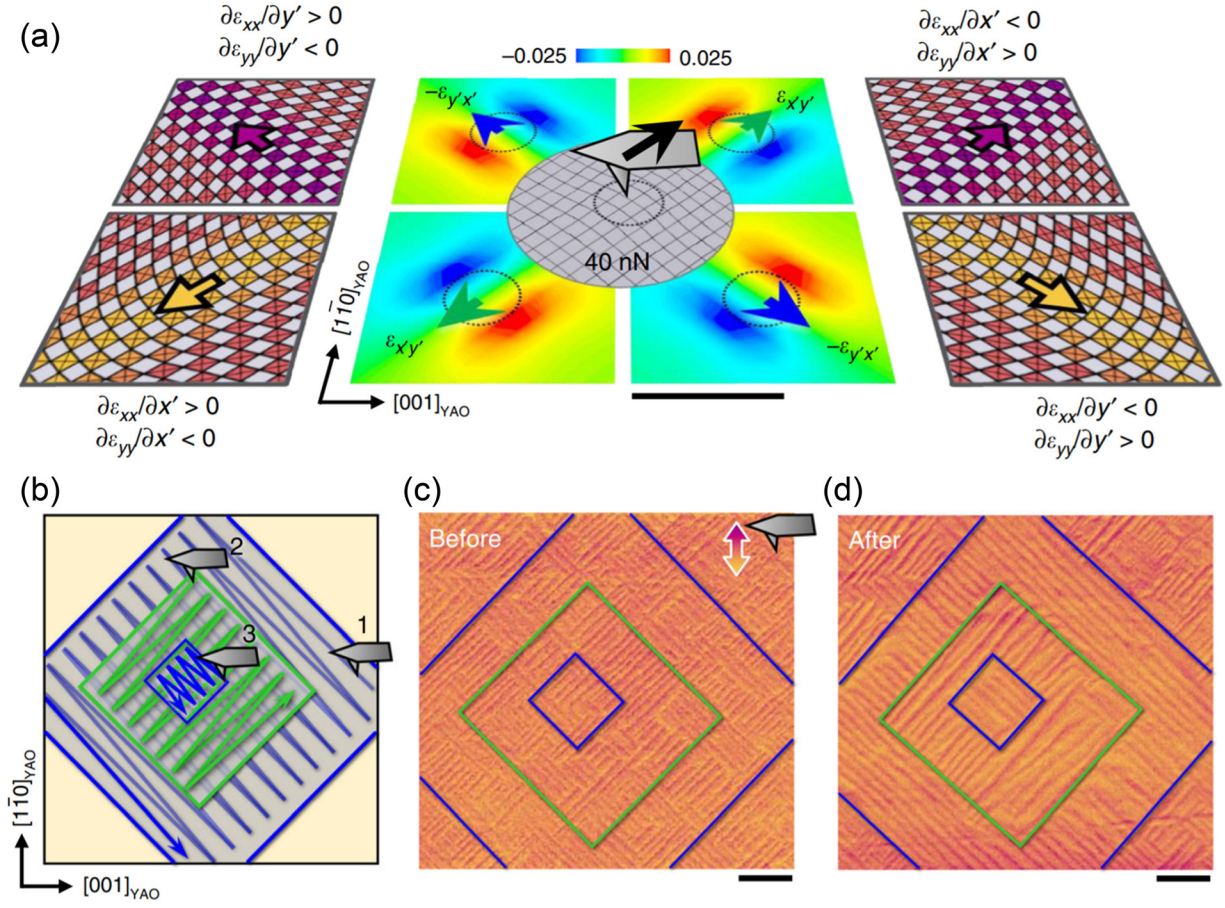

FIG. 8. Mechanical control of ferroelastic domain walls in WO_3 by AFM tip pressing and scanning. (a) The middle image shows the mechanical force-induced shear strain distribution, simulated by the finite-element modeling. Blue and green arrows indicate the AFM tip direction. Black scale bar represents 50 nm. The dashed circle represents the contact area of an AFM tip. Left and right schematics show the lattice deformations and flexoelectric polarizations of four-variant domain walls. The color contrasts (purple and yellow) indicate the macro-domain walls. (b) Three consecutive mechanical switchings through superimposed scans. Blue and green lines indicate the abbreviated trajectories of an AFM tip. The number represents the order of switching. (c, d) Lateral PFM images of the WO_3 domain walls (c) before and (d) after the mechanical switching. The color contrasts (purple and yellow) indicate the macro-domain walls. Scale bars represent 1 μm. Reproduced with permission from Yun *et al.*, Nat. Commun. **11**, 4898 (2020). Copyright 2020 Author(s), licensed under a Creative Commons Attribution 4.0 License.

for the contact mechanics of a piezoelectric half-space, which can be dominant due to the wetting of the film surface.[183,184] More importantly, most previous contact mechanics theories of piezoelectrics have not considered the flexoelectric coupling into the constitutive equations. The analytical solution with fully coupled piezoelectricity and flexoelectricity of a transversely isotropic half-space is given by Liu *et al.* for the indentation problem[185] and by Abdollahi *et al.* for modeling the mimicry piezoresponses of PFM due to flexoelectricity.[17]

In systems that can sustain large deformations, such as free-standing oxide membranes,[76,79,186–188] 2D materials,[75] and soft materials,[189] the evaluation of the finite strain gradients is of vital importance. This consideration is relevant to the recent finding of superelasticity in bent free-standing thin-film membranes of ferroelectrics oxides.[81,129,190] As the theory of flexoelectric systems subject to finite deformation has been established,[191,192] we expect it to be applied to understanding and exploring the AFM tip pressing-induced phenomena in free-standing oxide membranes and other flexible materials.

To conclude this subsection, we briefly remark on the choice of proper models for estimating the strain gradients under the AFM tip pressing. For most of the AFM tip pressing experiments, wherein the loading force is less than a few μN, the deformation of the thin film remains in the elastic regime, and the classical Hertz model can still serve as a good first approximation to the contact mechanics problem. Nevertheless, special care must be taken when the thin film is piezoelectrically active, or is highly anisotropic in physical properties, or is grown on a substrate with distinct mechanical behaviors. In these cases, a modified Hertz model with the specific conditions considered should be adopted to accurately acquire the strain gradient. For tip pressing-induced phenomena involving microstructure evolution (e.g., ferroic domain switching or phase transformation), the impact of the microstructure change on the strain gradient distribution should not be neglected, which usually requires a more comprehensive self-consistent model and numerical simulations. In addition, frictional forces associated with tip scanning can break the axis symmetry of the strain field of the static loading and significantly modify the strain-gradient distribution. More comprehensive theoretical models incorporating the nature of the contact and the multiple physical properties of materials are expected to quantify the strain gradients in more complicated systems and capture the associated kinetic processes therein.

V. RECENT PROGRESS

A. Ferroelectric domain engineering

The advancement of SPM techniques offers precise mechanical control of the desired area. A crude estimation shows that applying

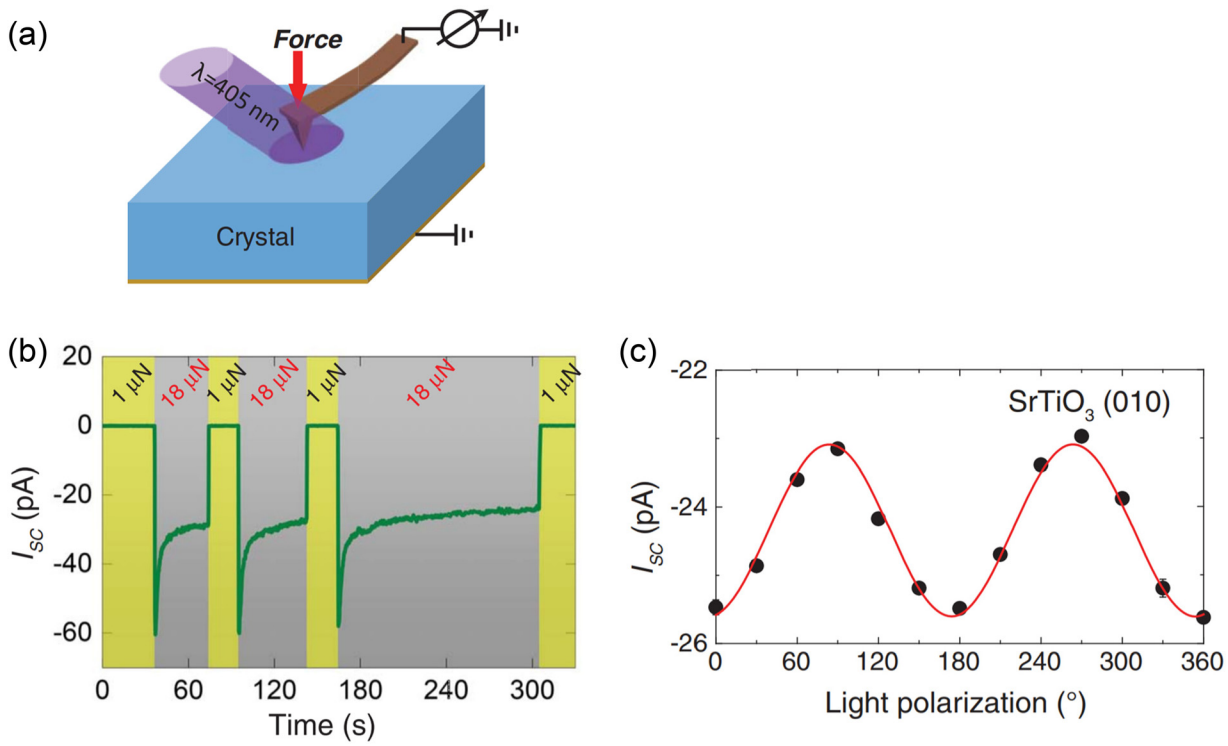

FIG. 9. Flexo-photovoltaic effect via AFM tip pressing. (a) Schematic illustrating illumination around the AFM tip-pressed area. A conductive AFM tip applies a local force on the surface of an originally centrosymmetric sample and simultaneously collects the resultant photovoltaic current under illumination with a laser of 405 nm wavelength. (b) Evolution of the photocurrent induced and collected by a conductive AFM tip with a high loading force on $SrTiO_3$. $SrTiO_3$ originally do not exhibit the bulk photovoltaic effect because it is centrosymmetric. However, with illumination around the AFM tip-pressed area on the $SrTiO_3$ surface, a large current under zero bias [i.e., short-circuit current (I_{SC})] is observed as the loading force is increased from 1 to 18 μN. (c) Light polarization dependence of the AFM tip pressing-induced I_{SC} measured on $SrTiO_3$. The red line is the fit to the equation $I_{SC} = \frac{\pi}{2} I_0 (A_z + B_z \cos 2\alpha)$, where I_0 is a light intensity, A_z and B_z are effective bulk photovoltaic coefficients of the locally deformed crystal, and α is the polarization angle of the incident light with respect to the top surface edge. Reproduced with permission from Yang *et al.*, Science **360**, 904–907 (2018). Copyright 2018 American Association for the Advancement of Science.

force of a few μN through a rigid and sharp tip onto an oxide surface can generate stress of several GPa, which decays in tens of nanometers from the center of the contact area. The highly concentrated stress field created directly interacts with the ferroelectric polarization through both piezoelectric and flexoelectric effects. In particular, when pressed by an AFM tip, ultrathin ferroelectric films experience compressive strains in both the longitudinal and transverse directions. In this situation, ferroelectric coercivity would decrease, so the strain gradient resulting from AFM tip pressing could effectively induce switching of ferroelectric polarization. In 2012, Lu *et al.* first demonstrated that by virtue of flexoelectricity, it is possible to switch ferroelectric polarization through around 1 μN mechanical load from an AFM tip in ultrathin $BaTiO_3$ film (Fig. 4).[57] After that, similar mechanical control of ferroelectric polarization has been reproduced in a various range of ferroelectric thin films (Fig. 5), such as $BaTiO_3$ (even with a top electrode),[57,59,61,193] $PbTiO_3$,[62] $Pb(Zr,Ti)O_3$,[58] nanopolar regions in $SrTiO_3$,[63] Al-doped HfO_2,[131] ferroelectric polymers PVDF-TrFE,[133] multiferroic $BiFeO_3$,[64,90,194] $TbMnO_3$,[195] and $Bi_5Ti_3FeO_{15}$.[120] Furthermore, attempts have been made to utilize mechanical control of polarization for ferroelectric nanodomain lithography in capacitor geometry. Specifically, Lu *et al.* demonstrated the local writing of ferroelectric polarization from upward to downward in Graphene/$BaTiO_3$/$La_{0.67}Sr_{0.33}MnO_3$/$SrTiO_3$ heterostructure.[193] This is not possible with electrical writing and even allows mechanical gates of top-electrode materials, such as graphene deposited on top of ferroelectrics (Fig. 6).[196]

Despite its great potential, AFM tip pressing usually allows for switching ferroelectric polarization only in a unidirectional way, that is, from upward to downward. However, recent experiments have somewhat overcome this limitation by demonstrating mechanical control of multiple polarization domains (Fig. 7)[64] or domain walls (Fig. 8)[197] in multiaxial ferroic materials. In particular in multiaxial ferroelectric materials, such as $BiFeO_3$, multiple domain switching pathways can be selectively controlled by an AFM tip motion-induced trailing flexoelectric field [Fig. 7(a)]. In other words, controlling the direction of tip motion results in a different direction of the last flexoelectric field, affecting domain switching. This so-called trailing flexoelectric field enables selective control of ferroelectric switching pathways in $BiFeO_3$.

Although the above study using $BiFeO_3$ demonstrates how to selectively control multiple ferroelectric switching pathways mechanically, the out-of-plane polarization still greatly favors the downward direction under AFM tip pressing. This strong preference has prevented reversible mechanical switching of ferroelectric polarization. It might be possible to achieve reversible pure in-plane polarization switching via a trailing flexoelectric field, for example, in much thinner $BiFeO_3$ films or materials with pure in-plane polarization such as Bi_2WO_6.[198]

The mechanical approach to switching ferroelectric polarizations circumvents voltage-induced side effects, such as leakage, charge injection, Joule heating, and dielectric breakdown. Moreover, mechanically written nanodomain arrays are spatially denser than the electrically induced counterparts,[57,133] while exhibiting comparable response time and retention properties.[64,65] These features of mechanical switching offer a new perspective for designing low-energy ultrahigh-density memories.

B. Emergent phenomena due to the broken inversion symmetry

One of the key features of the flexoelectric effect is that it can universally break inversion symmetry in arbitrary materials. With this special characteristic, it is possible to generate phenomena that otherwise only arise in non-centrosymmetric materials, in centrosymmetric materials, for example, creating pseudo-piezoelectricity using centrosymmetric materials.[199,200] Similarly, this spontaneous inversion symmetry breaking effect makes AFM tip pressing a perfect platform to manipulate physical properties in what were initially centrosymmetric materials. Yang *et al.* have shown a representative example of emergent phenomena due to the symmetry breaking by AFM tip pressing.[71] In their experiment, the large strain gradient generated by AFM tip pressing and the illumination with a laser of 405 nm wavelength were simultaneously applied onto centrosymmetric single crystals, as shown in Fig. 9(a). The result, as shown in Fig. 9(b), suggests that a significant

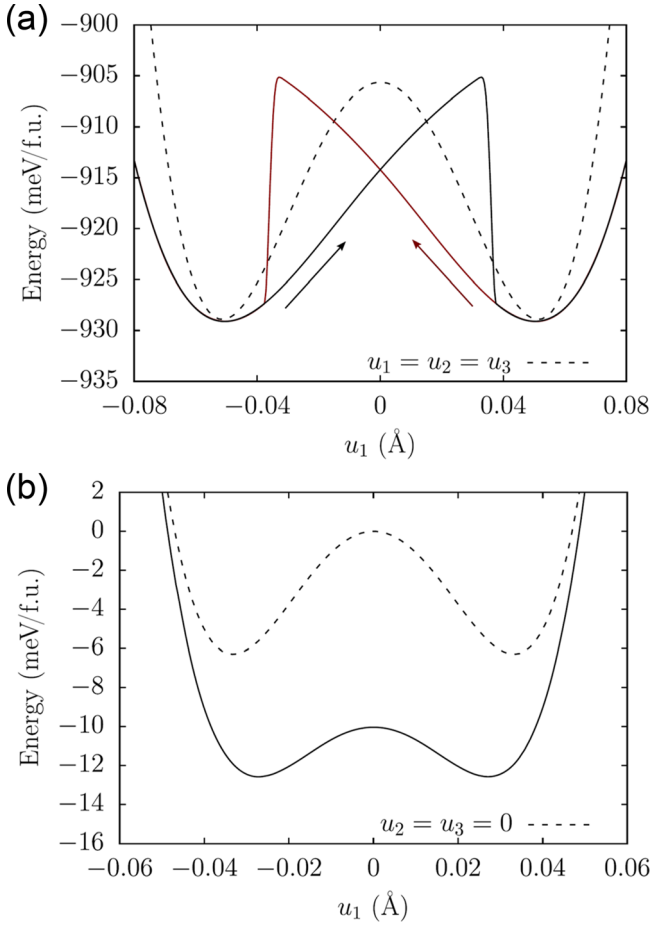

FIG. 10. Possible mechanical switching of a polar metal. Potential energy landscape for (a) $LiOsO_3$ and (b) $BaTiO_3$ based on first-principles effective Hamiltonians, obtained by minimizing the energy at a fixed polar mode u_1. For $LiOsO_3$, a double-well-like curve is obtained under the constraint $u_1 = u_2 = u_3$ [dashed line in (a)] and a butterfly-like diagram is obtained when all the parameters can evolve freely [solid line, colors, and arrows in (a) are used to illustrate the switching path]. For $BaTiO_3$, the dashed and solid lines in (b) represent the result under the constraint $u_2 = u_3 = 0$ and with no constraints, respectively. It is found that the mechanical switching of polarity is achievable in polar metals, as in conventional ferroelectrics. Reproduced with permission from Zabalo *et al.*, Phys. Rev. Lett. **126**, 127601 (2021). Copyright 2021 American Physical Society.

photocurrent was induced by the applied mechanical force even though the bulk photovoltaic effect can appeal only in non-centrosymmetric materials.

Yang *et al.* named this phenomenon as the flexo-photovoltaic effect.[71] The mechanism of the flexo-photovoltaic effect could be essentially the same as that of the bulk photovoltaic effect. The bulk photovoltaic effect originates from the asymmetric distribution of photoexcited nonequilibrium carriers in momentum space, caused by the absence of centrosymmetry in the material. Owing to universality of flexoelectricity, however, the flexo-photovoltaic effect might be distinctly advantageous over a typical bulk photovoltaic effect, as the centrosymmetry of any materials can be artificially broken by the applied strain gradient. The application of a sufficiently large strain gradient would generate a large flexoelectric polarization, which may lead to a high photocurrent and a good power conversion efficiency in the flexo-photovoltaic effect. For example, Yang *et al.* found that AFM tip pressing with a loading force of $\sim$15 μN could generate a local strain gradient as large as $\sim 10^7$ m^{-1} and then lead to a substantial photocurrent of a few A cm^{-2}.[71] In addition, the generation of such photocurrent was proved to only originate from the flexo-photovoltaic effect rather than from other factors, such as Schottky contact [Fig. 9(c)]. Also, when the material dimension is decreased into the nanoscale, this flexo-photovoltaic effect can obviously be improved. This study suggests that the application of flexoelectricity is an effective route to improve the performance of solar cells and optoelectronic devices.

In terms of broken inversion symmetry, a new class of materials has recently emerged, namely, polar (or ferroelectric) metals.[201] These materials have attracted a great deal of attention, as the unusual coexistence of metallicity and polarity promises novel physical and functional phenomena. One of the most fundamental questions about polar metals has been whether their polarity could be controlled by an external field. Since free charge carriers in the bulk screen the electric field, it is generally not possible to switch the polarity by applying an external electric field. On the other hand, the application of a strain gradient could be a feasible alternative to switch the polarity in polar metals due to the universal characteristic of flexoelectricity. A recent theoretical study has indeed revealed that flexoelectricity can be effectively used to mechanically switch the polarity of polar metals, such as the well-known polar metal $LiOsO_3$ (Fig. 10).[46] Importantly, flexoelectric effects in metals have been suggested to be comparable in magnitude to those of high k dielectrics.[202] Therefore, AFM tip pressing could be applied to polar metals to mechanically switch their polarity. Once the polarity is switched, it might be detected via other AFM modes, such as electrostatic force microscopy.[203]

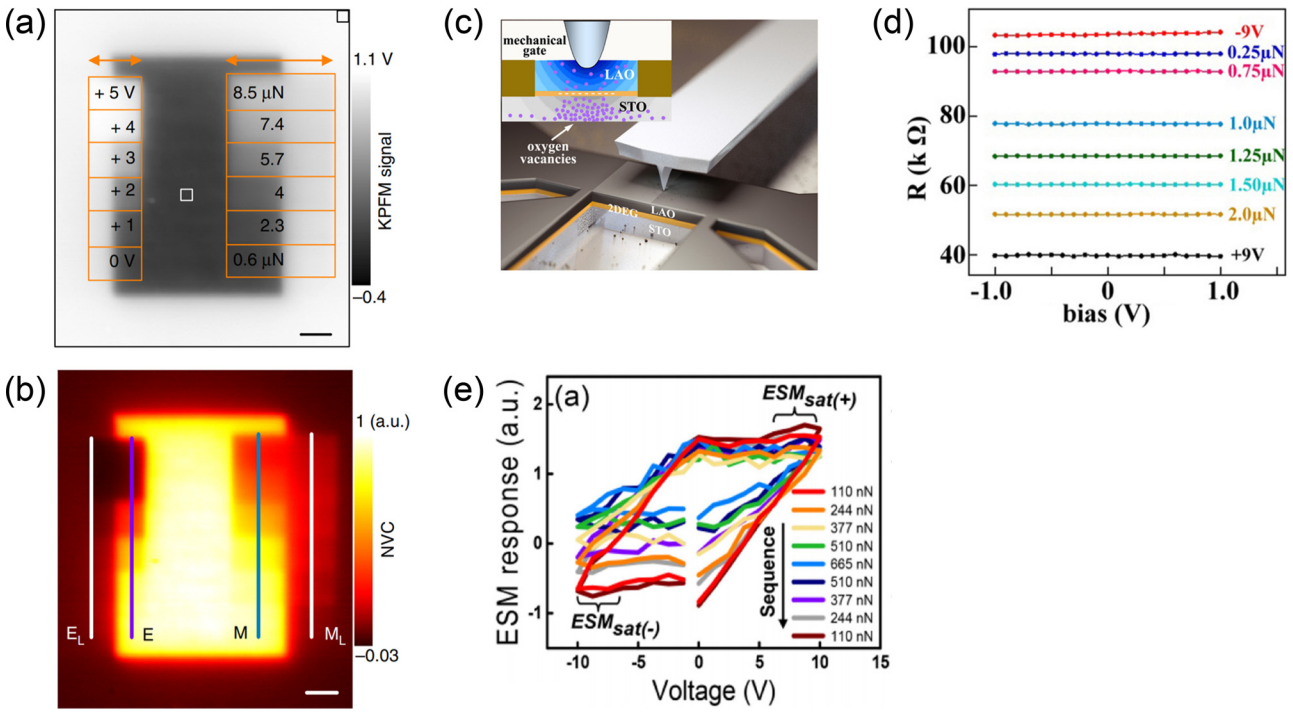

FIG. 11. Flexoelectricity-based defect migration via AFM tip pressing. (a) The Kelvin probe force microscope (KPFM) image after electrical and mechanical scans was performed across borders between the oxygen vacancy-enriched and pristine regions of $SrTiO_3$. (b) The normalized vacancy concentration map is constructed from the KPFM image in (a). Reproduced with permission from Das *et al.*, Nat. Commun. **8**, 615 (2017). Copyright 2017 Author(s), licensed under a Creative Commons Attribution 4.0 License. (c) Schematic of the structure used for investigation of the tip-induced stress effect on two-dimensional electron gas conductivity at $LaAlO_3/SrTiO_3$ interface. (d) Bias dependence of the $LaAlO_3/SrTiO_3$ interface resistance as a function of mechanical loads exerted by a grounded AFM probe. Reproduced with permission from Sharma *et al.*, Nano Lett. **15**, 3547–3551 (2015). Copyright 2015 American Chemical Society. (e) Averaged electrochemical strain microscopy hysteresis loops as a function of the applied force obtained by the continuous force waveform of dynamic force-modulated electrochemical strain microscopy. Reproduced with permission from Seol *et al.*, Nanotechnology **29**, 275709 (2018). Copyright 2018 IOP Publishing.

C. Defect migration due to flexoelectricity using AFM tip pressing

The flexoelectric field refers to an effective electric field in the materials due to a mechanical strain gradient. The flexoelectric field has been frequently used to evaluate the strength of flexoelectricity.[57,64] By the definition of flexoelectricity, a strain gradient can act as a driving force to generate electric polarization. This driving force could be expressed as $f \times (\partial\varepsilon/\partial x)$, where f is the flexocoupling coefficient with the unit of V and $\partial\varepsilon/\partial x$ is the strain gradient with the unit of m^{-1}. Since the driving force of polarization has the same SI unit ($V\ m^{-1}$) as an electric field, it is convenient to equate the strain gradient to a local effective electric field. Nevertheless, the flexoelectric field defined in this sense is unable to become a macroscopic electric field, since in general, it is not curl-free and cannot be linked with electrostatic potential.[27,30] Therefore, it is irrational to maintain that the flexoelectric field can act on charged species as a real macroscopic electric field. However, a strain gradient changes not only the ionic lattices but also the electronic structures. The resultant local charge redistribution gives rise to a variation of local electric fields. Consequently, this depolarization field can act on the charged entities such as oxygen vacancy, electron and holes, and doping elements.

For example, Das *et al.* applied a mechanical force with an AFM tip to dynamically reconfigure the surface oxygen vacancy distribution in a non-ferroelectric $SrTiO_3$ thin film [Figs. 11(a) and 11(b)].[67] With the help of the phase–field simulation method, the main driving force is attributed to the depolarization field generated by flexoelectricity. Also, possible controllability of the amount of oxygen vacancy migration by AFM tip pressing is suggested by tailoring the distribution of the depolarization field with the tuning of the tip shape from sharp to blunt. Similar pressure-induced migration of charged defects in oxides has also been evident in tuning the $LaAlO_3/SrTiO_3$ interface conductivity [Figs. 11(c) and 11(d)][66,204] and switching the electroresistance in non-stoichiometric NiO films [Fig. 11(e)].[96,205]

D. Conductivity change induced by flexoelectricity

When the film is sufficiently thin, electrons could experience quantum tunneling across the film. Moreover, the amount of electron tunneling can be tuned by tailoring the magnitude or the direction of the internal field. The most representative example of the control of tunnel current can be seen in the ferroelectric tunnel junction (FTJ).[206–211] The basic working principle of the FTJ is that the application of an electric field through a metal/ferroelectric/metal junction changes the direction of ferroelectric polarization in ultrathin ferroelectric film, resulting in variation in the tunnel electroresistance of the film. The imperfect screening of polarization charges at the interface gives rise to an uneven potential profile whose asymmetry and average height can be dependent on the polarization direction.

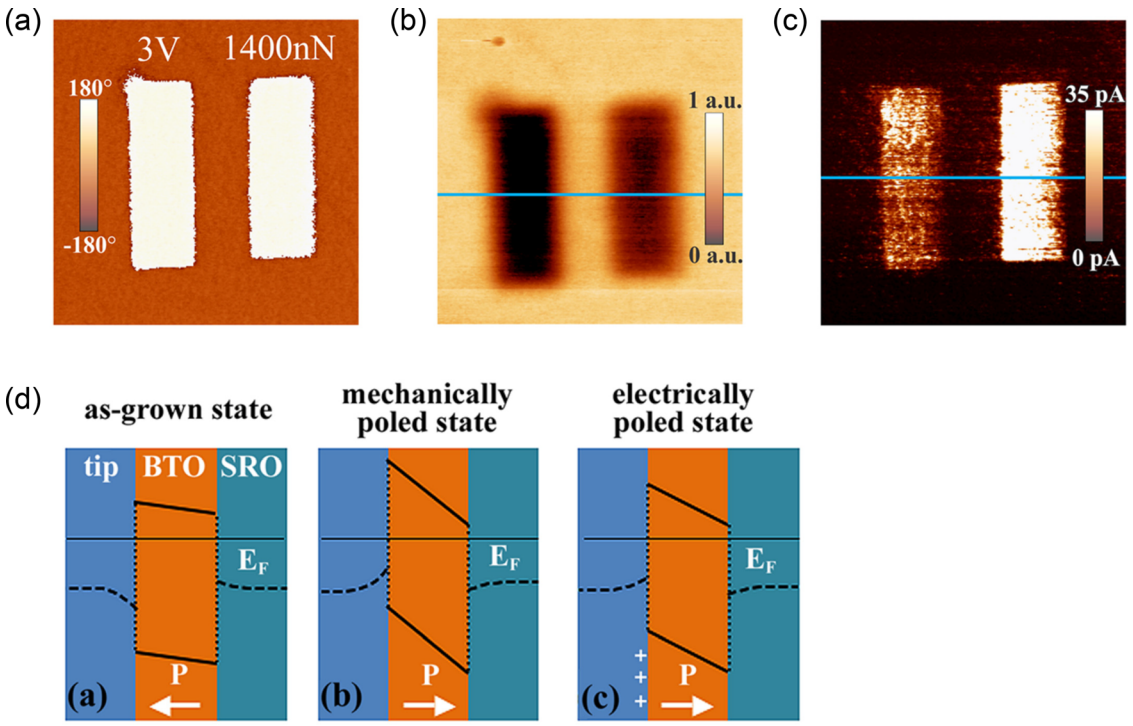

FIG. 12. Flexoelectricity-induced conductivity change via AFM tip pressing. (a) PFM phase image of ultrathin $BaTiO_3$ film after the generation of the downward-oriented domains by electrical poling (left) and mechanical loading force (right). (b) Electrostatic force microscopy image was taken at the same location as in (a). (c) Tunneling current map acquired in the conductive AFM mode at the same location as in (a) and (b). (d) Schematic band diagrams of the ferroelectric tunnel junction formed by the $BaTiO_3$ film sandwiched between the bottom $SrRuO_3$ electrode and a conductive AFM tip. Reproduced with permission from Lu *et al.*, Nano Lett. **12**, 6289–6292 (2012). Copyright 2012 American Chemical Society.

Similar to the electric control on the FTJ, a mechanical force can be used to tune the tunnel electroresistance in an ultrathin ferroelectric film by virtue of flexoelectricity (Fig. 12).[212] Specifically, the mechanically induced tunneling electroresistance effect in ultrathin ferroelectric films is facilitated by flexoelectric switching of polarization due to the strain gradient developed by the AFM tip pressing. Moreover, voltage-free switching of polarization gives rise to an enhanced tunneling electroresistance effect, compared to that by electric bias, due to the steeper band bending resulting from lower screening charge density.

Furthermore, mechanical control of resistive switching in various materials by AFM tip pressing has been reported. One of the possible origins has been attributed to ionic diffusion due to the flexoelectricity together with the inverse Vegard effect.[61,66,95,96,204,213]

E. Tailoring band structure with flexoelectricity using AFM tip pressing

As the direction of ferroelectric polarization can change the tunnel electroresistance of the ultrathin ferroelectric film, the magnitude of electric polarization can also give rise to variation of the tunnel electroresistance. Similarly, the magnitude of flexoelectric polarization generated by AFM tip pressing on ultrathin films can also change the amount of band bending on the electronic structure of the films. When the amount of flexoelectric polarization becomes larger than a certain threshold value, the conduction band minimum of the material can go lower than the Fermi level of the material. In this case, electrons could accumulate in those regions and could decrease the effective barrier width, while the effective barrier height remains almost the same. This could yield a significant variation in tunneling current spectra.

This idea was recently investigated by applying strain gradients with an AFM tip to an archetypical $SrTiO_3$ ultrathin film and simultaneously measuring the tunnel current across it.[68] Indeed, a notable modulation in current–voltage (I–V) spectra has been experimentally observed in $SrTiO_3$ ultrathin film as the applied AFM tip pressure changes (Fig. 13). Specifically, the measured tunnel current exhibits critical behavior as a function of strain gradients, which manifests large modification of tunnel barrier profiles via flexoelectricity. Additional investigation of this critical behavior shows considerably enhanced

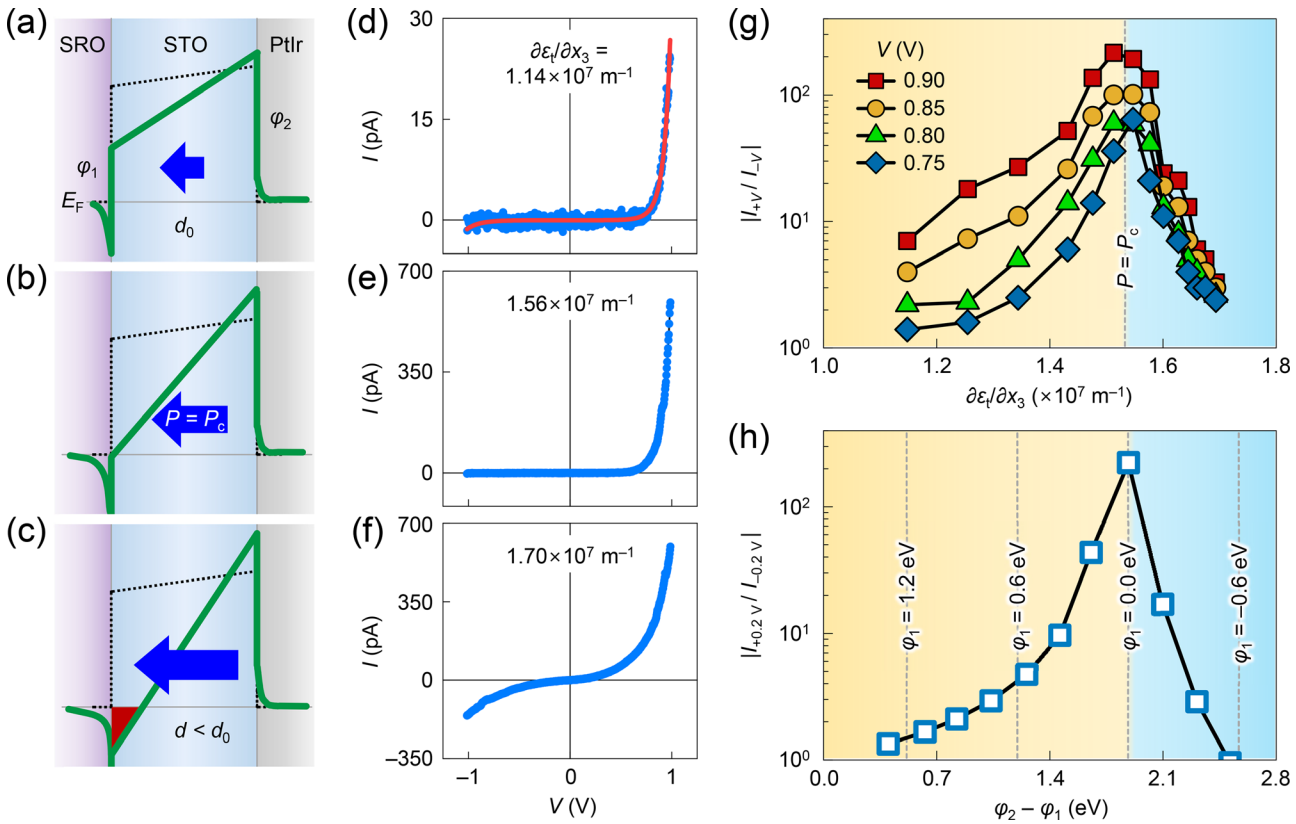

FIG. 13. Flexoelectrically tuned tunneling transport via AFM tip pressing. (a)–(c) Schematics of the potential energy profile across $SrTiO_3$ with increasing flexoelectric polarization (P; blue arrows). An additional electrostatic potential by P modifies the original barrier potential energy (dotted black) into the total potential energy (solid green). At a critical polarization P_c, the tunnel barrier becomes triangular with $\varphi_1 = 0$ and $\varphi_2 = \varphi_{0,2} + \varphi_{0,1}\cdot(\delta_{Ptlr}/\delta_{SRO})$. (d)–(f) Measured tunnel current (I) vs voltage (V) curves for three representative strain gradients in 9 unit cells-thick $SrTiO_3$. The solid red line indicates the fitted result. (g) The rectification ratios $|I_{+V}/I_{-V}|$ of the measured tunnel currents as a function of strain gradients. With increasing strain gradients, the tunneling I–V curves become more asymmetric in the yellow regime of strain gradients below 1.56 × 10^7 m^{-1}, whereas they become more symmetric in the blue regime. (h) The simulated $|I_{+V}/I_{-V}|$ at $V = 0.2$ V as a function of φ_2–φ_1. Reproduced with permission from Das *et al.*, Nat. Commun. **10**, 537 (2019). Copyright 2019 Author(s), licensed under a Creative Commons Attribution 4.0 License.

flexocoupling strength in ultrathin $SrTiO_3$, compared to that in bulk, rendering flexoelectricity more potent at the nanoscale.

Furthermore, an AFM tip-induced flexoelectric internal field could be large enough to allow the electrical-state switching in dielectrics[68,69] and semiconductors.[22] It has long remained difficult to control the electrical states (i.e., insulating and conducting states) in an originally highly insulating dielectric; under weak electric fields, dielectrics exhibit negligibly low conductivity, whereas, under strong fields, they incur irreversible damage. However, flexoelectricity challenges this long-standing belief. When the strain gradient-induced flexoelectric polarization reaches a threshold value, a strong depolarization field could make both the conduction band minimum and valence band maximum cross the Fermi level. This band crossing might promote interband tunneling between the valence and conduction bands, causing Zener breakdown,[214,215] which accounts for the insulating-to-conducting transition in a dielectric (Fig. 14).[69] Importantly, this approach generally enables the application of a nondestructive, strong electrostatic field in insulators. Furthermore, when applied to semiconductors, the AFM tip-induced flexoelectric field could serve as an active "gate" for modulating the metal–semiconductor interface Schottky barrier and controlling charge–carrier transport (Fig. 15).[22] These active electronics based on various semiconductors were found to guarantee fast response and high resolution. Therefore, the scope of electric control in solids, such as dielectrics and semiconductors, could be extended to explore unconventional electronic phenomena under strong static fields via flexoelectricity.

VI. CONCLUSION AND PERSPECTIVES

We would like to emphasize that nanoscale flexoelectricity could be more powerful than previously expected. It was thought that the enhanced flexoelectric effect at the nanoscale naturally originates from the increased strain gradients, as strain gradients are inversely proportional to the length scale. In this regard, AFM tip pressing has been extensively utilized as an effective experimental tool to induce huge strain gradients at the nanoscale. However, this AFM tip pressing method has more recently also discovered a greater, previously hidden potential of nanoscale flexoelectricity.[22,68,76] Two independent studies, one based on electrical measurements[68] and the other on purely elastic measurements,[76] have consistently shown that the flexocoupling coefficient itself of $SrTiO_3$ can be improved by one order of magnitude

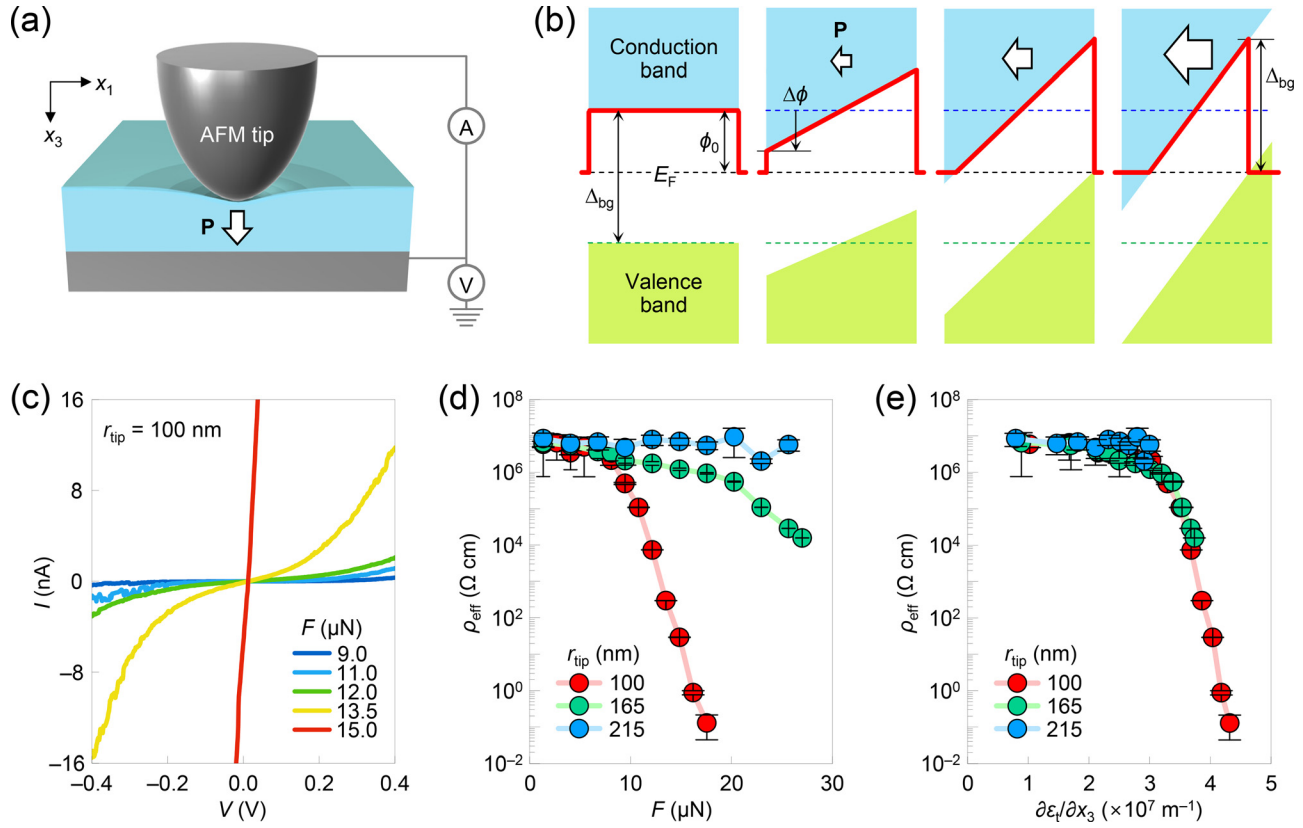

FIG. 14. Colossal flexoresistance effect via AFM tip pressing. (a) Schematic of the experimental setup, illustrating the flexoelectric polarization (**P**; white arrow) generated by AFM tip pressing the surface of ultrathin dielectrics. While generating large strain gradients, the tunneling currents are simultaneously measured across the flexoelectrically polarized $SrTiO_3$. (b) Schematic of the potential energy profiles across $SrTiO_3$ with increasing flexoelectric polarization. Red solid lines and black dashed lines indicate the effective tunnel barrier and Fermi level, respectively. Blue and green dashed lines indicate the conduction band minimum and valence band maximum for $\mathbf{P} = 0$, respectively. (c) Current–voltage (I–V) curves were obtained by conductive AFM measurements in a 10 unit cell-thick $SrTiO_3$ film upon application of various tip loading forces. Five representative curves are shown here. (d) Effective resistivity (ρ_{eff}) as a function of tip loading force. (e) ρ_{eff} as a function of the AFM tip-induced transverse strain gradient $\partial u_t/\partial x_3$. Reproduced with permission from Park *et al.*, Nat. Commun. **11**, 2586 (2020). Copyright 2020 Author(s), licensed under a Creative Commons Attribution 4.0 License.

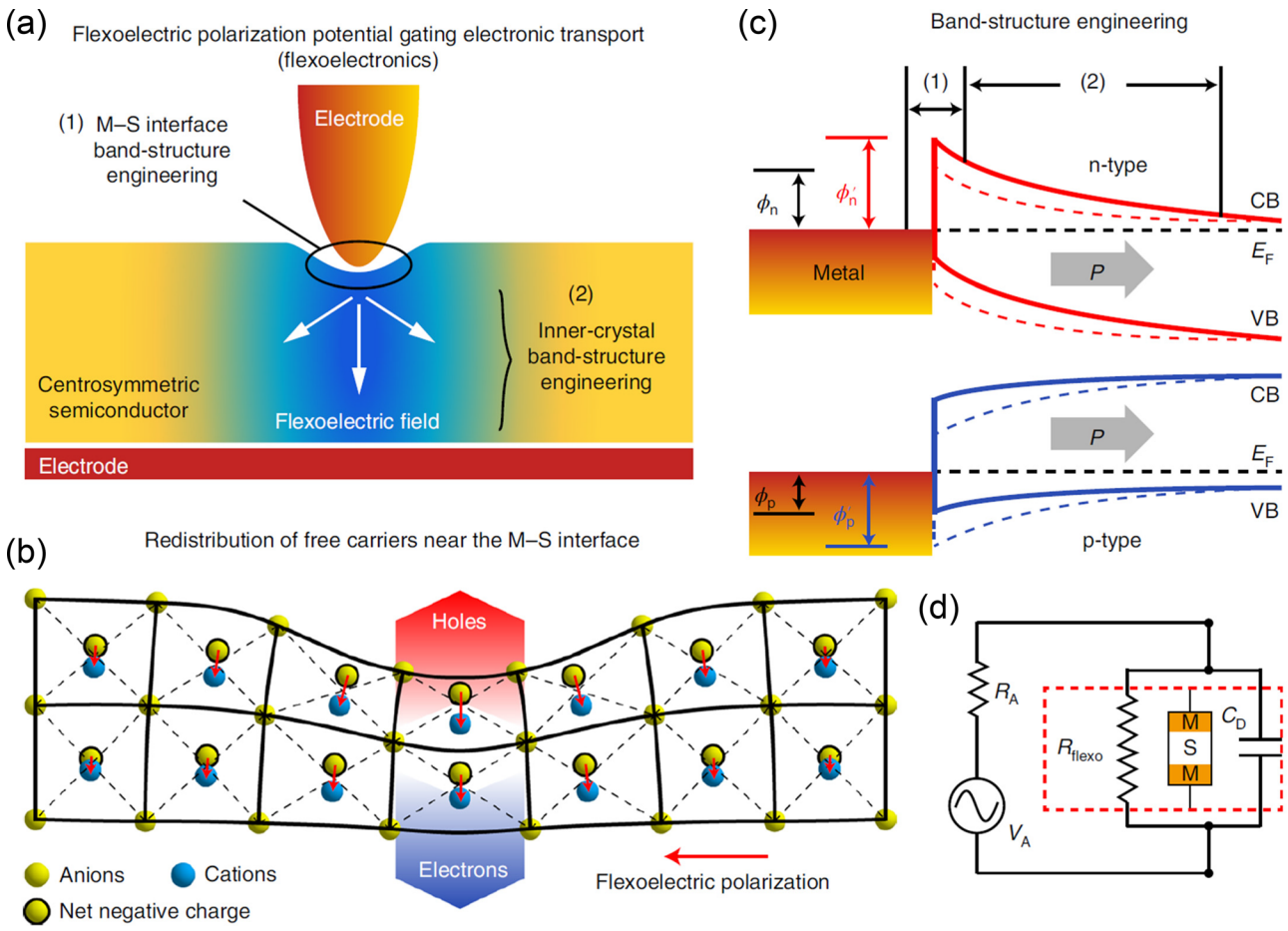

FIG. 15. Flexoelectronics via AFM tip pressing. (a) Schematic showing the concept of flexoelectronics, according to which the flexoelectric-polarization potential generated in a centrosymmetric semiconductor gates the electronic transport. (b) Inhomogeneous strained centrosymmetric crystal structure. (c) A flexoelectric built-in electric field formed in a centrosymmetric semiconductor exerts a substantial influence on the concentration and distribution of free carriers near the interface, resulting in band structure engineering. ϕ_n/ϕ'_n and ϕ_p/ϕ'_p represent the Schottky barrier heights formed between a metal and n-type and p-type semiconductor contacts without (dashed line) and with (solid line) strain, respectively. (d) Equivalent circuit diagram for the flexoelectronics. Reproduced with permission from Wang *et al.*, Nat. Nanotechnol. **15**, 661–667 (2020). Copyright 2020 Springer Nature.

under huge strain gradients at the nanoscale. Although more detailed theoretical studies of microscopic origin are required, these results suggest that flexocoupling coefficients can exceed Kogan's phenomenological estimate (i.e., 1–10 V).[11,31] Therefore, huge strain gradients at the nanoscale could, in turn, enhance the flexocoupling coefficient, promising a much stronger nanoscale flexoelectric effect and its application potential.

In addition, it would be worth discussing a possible beneficial contribution of strains that coexist with strain gradients in AFM-based experiments. AFM tip pressing generates not only strain gradients but also considerable longitudinal compressive strains [Figs. 16(a) and 16(b)], even above several percent. It is fundamentally important to distinguish the strain gradient-induced effect from the strain-induced effect, so we have presented some relevant methods for this. However, a certain technological potential of flexoelectricity could greatly benefit from such coexistence of strain gradient and strain. For example, AFM tip-induced strain could beneficially reduce ferroelectric coercivity and the associated threshold loading force required for mechanically switching ferroelectric polarization [Fig. 16(c)].[64] The low threshold loading force guarantees energy-efficient polarization switching[126] and might increase the density of written nanodomains due to the decreased tip–sample contact area. When employing complex ferroelectrics,[216–218] the AFM tip-induced strains might also more significantly lower the ferroelectric coercivity, due to the possible existence of metastable states. Furthermore, not only for this mechanical switching of polarization, the AFM tip-induced strains could be beneficial for largely controlling the local free energy landscape of complex materials. Therefore, by combining the effects from strain gradient and strain, we might access fascinating metastable quantum states and even write them locally at the nanoscale.

Finally, we would like to mention some of the future research directions to pursue. AFM is a perfect tool to exploit the strong scaling characteristic of flexoelectricity. Even though there have recently been extensive studies related to flexoelectricity using this technique, there

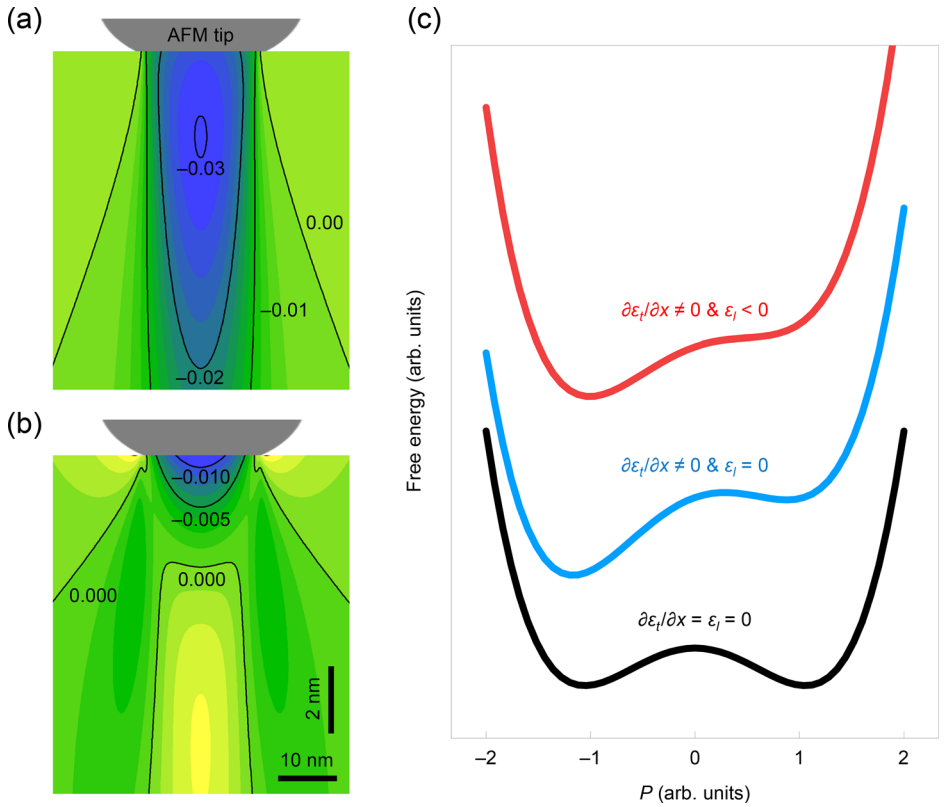

FIG. 16. Coexistence of strain and strain gradient under AFM tip pressing. (a) Longitudinal strain ε_l under AFM tip loading force of 800 nN, which shows a rather homogeneous distribution, yielding a net compressive strain. (b) Transverse strain ε_t under AFM tip loading force of 800 nN, which shows a quite inhomogeneous distribution, yielding a considerable strain gradient. In (a) and (b), spatial distributions of strain induced by a spherical indenter have been calculated analytically with the Hertzian contact model and the Boussinesq's calculation.[151] We set the contact radius, Poisson ratio, and Young's modulus to be 10 nm, 0.22, and 100 GPa, respectively. (c) Free energy landscapes for a ferroelectric without strain and strain gradient (black), with a transverse strain gradient $\partial\varepsilon_t/\partial x$ (blue), and with a transverse strain gradient $\partial\varepsilon_t/\partial x$ and compressive longitudinal strain ε_l (red).

can still be many more interesting research topics that can be further studied with this technique. First, the inversion symmetry can be used to generate spin band splitting, especially in a material with strong spin–orbit coupling, resulting in exotic electronic states and novel spintronic functionalities.[219–224] Therefore, AFM tip pressing could serve as a source to generate local inversion symmetry breaking to study the Rashba-type effects, the generation of magnetic skyrmions on centrosymmetric materials,[225] and so on. Second, the AFM tip pressing method is advantageous in studying rich flexoelectricity-driven phenomena in 2D materials, including 2D van der Waals crystals and oxide membranes. When 2D materials are placed on a holey substrate,[226] AFM tip pressing could systematically generate strain gradients onto them. Furthermore, by applying an electric field and then generating local nanobubbles in 2D materials via the AFM tip, it is even possible to create permanent nanostructures with large strain gradients.[77] These strain gradients could universally allow for polar symmetry-related functionalities, such as piezoelectricity and nonlinear optical responses, in 2D materials. They could also be exploited to break inversion symmetry and tailor the bandgap opening in topological materials like graphene,[227–230] which is essential for designing novel electronic devices.[231]

To sum up, we provide basic working principles of AFM tip pressing and methods of how to estimates strain gradients generated by the tip pressing. Also, we summarize recent research progress in AFM tip pressing-based flexoelectricity and provide future research direction on this research area. AFM tip-based applications (e.g., data storage) have potentially promised ultra-high storage density with bit sizes even down to the atomic scale.[232] The feasibility of the AFM tip-based practical device applications depends not only on their storage density but also on many other factors, including cost, market demand, and the emergence of new applications. We expect that research on nanoscale flexoelectricity, which has recently been in the spotlight, will further improve the prospects for AFM tip-based device applications.

ACKNOWLEDGMENTS

This work was supported by the Research Center Program of the IBS (Institute for Basic Science) in Korea (Grant No. IBS-R009-D1) and by the National Research Foundation of Korea (NRF) grant funded by the Korea government (MSIT) (Nos. 2018R1A5A6075964, 2019R1C1C1002558, and 2021R1A5A103299611). This work was supported by Samsung Electronics Co., Ltd (No. IO201211–08061-01). S.M.Y. acknowledges the support by the National Research Foundation of Korea (NRF) grant funded by the Korea government (MSIT) (No. NRF-2019R1A2C1085812). S.M.Y. also acknowledges the supports by MOTIE (Ministry of Trade, Industry and Energy) (No. 10080657) and the KRSC (Korea Semiconductor Research Consortium) support program for the development of future semi-conductor devices. B.W. and L.Q.C. acknowledge the support from the U.S. National Science Foundation under the Grant No. DMR-1744213.

AUTHOR DECLARATIONS

Conflict of Interest

The authors declare no competing interest.

Author Contributions

S.M.P. and B.W. contributed equally to this work.

DATA AVAILABILITY

Data sharing is not applicable to this article as no new data were created or analyzed in this study.

REFERENCES

[1]G. Binnig, H. Rohrer, C. Gerber, and E. Weibel, Phys. Rev. Lett. **49**, 57 (1982).
[2]G. Binnig, C. F. Quate, and C. Gerber, Phys. Rev. Lett. **56**, 930 (1986).
[3]S. V. Kalinin and D. A. Bonnell, Phys. Rev. B: Condens. Matter Mater. Phys. **65**, 125408 (2002).
[4]A. Gruverman and S. V. Kalinin, J. Mater. Sci. **41**, 107 (2006).
[5]D. A. Bonnell, S. V. Kalinin, A. L. Kholkin, and A. Gruverman, MRS Bull. **34**, 648 (2009).
[6]M. P. Murrell, M. E. Welland, S. J. O'Shea, T. M. H. Wong, J. R. Barnes, A. W. McKinnon, M. Heyns, and S. Verhaverbeke, Appl. Phys. Lett. **62**, 786 (1993).
[7]E. A. Eliseev, A. N. Morozovska, M. D. Glinchuk, and R. Blinc, Phys. Rev. B **79**, 165433 (2009).
[8]P. Lukashev and R. F. Sabirianov, Phys. Rev. B **82**, 094417 (2010).
[9]E. A. Eliseev, M. D. Glinchuk, V. Khist, V. V. Skorokhod, R. Blinc, and A. N. Morozovska, Phys. Rev. B **84**, 174112 (2011).
[10]J. X. Zhang, R. J. Zeches, Q. He, Y. H. Chu, and R. Ramesh, Nanoscale **4**, 6196 (2012).
[11]S. M. Kogan, Sov. Phys. Solid State **5**, 2069 (1964).
[12]J. Y. Fu, W. Zhu, N. Li, and L. E. Cross, J. Appl. Phys. **100**, 024112 (2006).
[13]J. Y. Fu and L. E. Cross, Appl. Phys. Lett. **91**, 162903 (2007).
[14]L. Shu, F. Li, W. Huang, X. Wei, X. Yao, and X. Jiang, J. Appl. Phys. **116**, 144105 (2014).
[15]U. K. Bhaskar, N. Banerjee, A. Abdollahi, Z. Wang, D. G. Schlom, G. Rijnders, and G. Catalan, Nat. Nanotechnol. **11**, 263 (2016).
[16]S. Zhang, K. Liu, M. Xu, and S. Shen, Appl. Phys. Lett. **111**, 082904 (2017).
[17]A. Abdollahi, N. Domingo, I. Arias, and G. Catalan, Nat. Commun. **10**, 1266 (2019).
[18]P. Zubko, G. Catalan, A. Buckley, P. R. L. Welche, and J. F. Scott, Phys. Rev. Lett. **99**, 167601 (2007).
[19]D. Lee, A. Yoon, S. Y. Jang, J. G. Yoon, J. S. Chung, M. Kim, J. F. Scott, and T. W. Noh, Phys. Rev. Lett. **107**, 057602 (2011).
[20]J. Narvaez, F. Vasquez-Sancho, and G. Catalan, Nature **538**, 219 (2016).
[21]L. Shu, S. Ke, L. Fei, W. Huang, Z. Wang, J. Gong, X. Jiang, L. Wang, F. Li, S. Lei, Z. Rao, Y. Zhou, R.-K. Zheng, X. Yao, Y. Wang, M. Stengel, and G. Catalan, Nat. Mater. **19**, 605 (2020).
[22]L. Wang, S. Liu, X. Feng, C. Zhang, L. Zhu, J. Zhai, Y. Qin, and Z. L. Wang, Nat. Nanotechnol. **15**, 661 (2020).
[23]K. D. Breneman, W. E. Brownell, and R. D. Rabbitt, PLoS One **4**, e5201 (2009).
[24]F. Vasquez-Sancho, A. Abdollahi, D. Damjanovic, and G. Catalan, Adv. Mater. **30**, 1801413 (2018).
[25]S. V. Kalinin and V. Meunier, Phys. Rev. B: Condens. Matter Mater. Phys. **77**, 033403 (2008).
[26]D. Lee and T. W. Noh, Philos. Trans. R. Soc. A **370**, 4944 (2012).
[27]P. V. Yudin and A. K. Tagantsev, Nanotechnology **24**, 432001 (2013).
[28]T. D. Nguyen, S. Mao, Y. W. Yeh, P. K. Purohit, and M. C. McAlpine, Adv. Mater. **25**, 946 (2013).
[29]L. Shu, R. Liang, Z. Rao, L. Fei, S. Ke, and Y. Wang, J. Adv. Ceram. **8**, 153 (2019).
[30]B. Wang, Y. Gu, S. Zhang, and L. Q. Chen, Prog. Mater. Sci. **106**, 100570 (2019).
[31]P. Zubko, G. Catalan, and A. K. Tagantsev, Annu. Rev. Mater. Res. **43**, 387 (2013).
[32]Y. Heo, P. Sharma, Y. Y. Liu, J. Y. Li, and J. Seidel, J. Mater. Chem. C **7**, 12441 (2019).
[33]O. I. Bursian and E. V. Zaikovskii, Sov. Phys. Solid State **10**, 1121 (1968).
[34]V. L. Indenbom, E. B. Loginov, and M. A. Osipov, Sov. Phys. Crystallogr. **26**, 656 (1981).
[35]A. K. Tagantsev, Phys. Rev. B **34**, 5883 (1986).
[36]R. Maranganti and P. Sharma, Phys. Rev. B **80**, 054109 (2009).
[37]J. Hong, G. Catalan, J. F. Scott, and E. Artacho, J. Phys.: Condens. Matter **22**, 112201 (2010).
[38]R. Resta, Phys. Rev. Lett. **105**, 127601 (2010).
[39]J. Hong and D. Vanderbilt, Phys. Rev. B **88**, 174107 (2013).
[40]M. Stengel, Phys. Rev. B **90**, 201112(R) (2014).
[41]T. Hu, Q. Deng, X. Liang, and S. Shen, J. Appl. Phys. **122**, 055106 (2017).
[42]W. Ma and L. E. Cross, Appl. Phys. Lett. **88**, 232902 (2006).
[43]P. V. Yudin, R. Ahluwalia, A. K. Tagantsev, P. V. Yudin, R. Ahluwalia, and A. K. Tagantsev, Appl. Phys. Lett. **104**, 082913 (2014).
[44]W. Ma and L. E. Cross, Appl. Phys. Lett. **78**, 2920 (2001).
[45]W. Ma and L. E. Cross, Appl. Phys. Lett. **79**, 4420 (2001).
[46]A. Zabalo and M. Stengel, Phys. Rev. Lett. **126**, 127601 (2021).
[47]Y. Qi, J. Kim, T. D. Nguyen, B. Lisko, P. K. Purohit, and M. C. McAlpine, Nano Lett. **11**, 1331 (2011).
[48]M. S. Majdoub, P. Sharma, and T. Cagin, Phys. Rev. B **77**, 125424 (2008).
[49]G. Catalan, B. Noheda, J. McAneney, L. J. Sinnamon, and J. M. Gregg, Phys. Rev. B **72**, 020102 (2005).
[50]G. Catalan, A. Lubk, A. H. G. Vlooswijk, E. Snoeck, C. Magen, A. Janssens, G. Rispens, G. Rijnders, D. H. A. Blank, and B. Noheda, Nat. Mater. **10**, 963 (2011).
[51]A. Y. Borisevich, E. A. Eliseev, A. N. Morozovska, C. J. Cheng, J. Y. Lin, Y. H. Chu, D. Kan, I. Takeuchi, V. Nagarajan, and S. V. Kalinin, Nat. Commun. **3**, 775 (2012).
[52]P. Gao, S. Yang, R. Ishikawa, N. Li, B. Feng, A. Kumamoto, N. Shibata, P. Yu, and Y. Ikuhara, Phys. Rev. Lett. **120**, 267601 (2018).
[53]H. Wang, X. Jiang, Y. Wang, R. W. Stark, P. A. Van Aken, J. Mannhart, and H. Boschker, Nano Lett. **20**, 88 (2020).
[54]H. Simons, A. C. Jakobsen, S. R. Ahl, H. F. Poulsen, W. Pantleon, Y. H. Chu, C. Detlefs, and N. Valanoor, Nano Lett. **19**, 1445 (2019).
[55]A. Lubk, M. D. Rossell, J. Seidel, Y. H. Chu, R. Ramesh, M. J. Hÿtch, and E. Snoeck, Nano Lett. **13**, 1410 (2013).
[56]A. Schiaffino and M. Stengel, Phys. Rev. Lett. **119**, 137601 (2017).
[57]H. Lu, C. W. Bark, D. E. De Los Ojos, J. Alcala, C. B. Eom, G. Catalan, and A. Gruverman, Science **336**, 59 (2012).
[58]E. J. Guo, R. Roth, S. Das, and K. Dörr, Appl. Phys. Lett. **105**, 012903 (2014).
[59]W. Zheng, X. Qiu, C. Li, C. Zheng, X. Ge, A. Li, and D. Wu, Appl. Phys. Lett. **104**, 042907 (2014).
[60]D. Lee, H. Lu, Y. Gu, S. Y. Choi, S. D. Li, S. Ryu, T. R. Paudel, K. Song, E. Mikheev, S. Lee, S. Stemmer, D. A. Tenne, S. H. Oh, E. Y. Tsymbal, X. Wu, L. Q. Chen, A. Gruverman, and C. B. Eom, Science **349**, 1314 (2015).
[61]A. Gómez, J. M. Vila-Fungueiriño, R. Moalla, G. Saint-Girons, J. Gázquez, M. Varela, R. Bachelet, M. Gich, F. Rivadulla, and A. Carretero-Genevrier, Small **13**, 1701614 (2017).
[62]H. Lu, S. Liu, Z. Ye, S. Yasui, H. Funakubo, A. M. Rappe, and A. Gruverman, Appl. Phys. Lett. **110**, 222903 (2017).
[63]H. Lu, D. Lee, K. Klyukin, L. Tao, B. Wang, H. Lee, J. Lee, T. R. Paudel, L. Q. Chen, E. Y. Tsymbal, V. Alexandrov, C. B. Eom, and A. Gruverman, Nano Lett. **18**, 491 (2018).
[64]S. M. Park, B. Wang, S. Das, S. C. Chae, J. S. Chung, J. G. Yoon, L. Q. Chen, S. M. Yang, and T. W. Noh, Nat. Nanotechnol. **13**, 366 (2018).
[65]P. Sharma, S. Ryu, Z. Viskadourakis, T. R. Paudel, H. Lee, C. Panagopoulos, E. Y. Tsymbal, C. B. Eom, and A. Gruverman, Adv. Funct. Mater. **25**, 6538 (2015).
[66]P. Sharma, S. Ryu, J. D. Burton, T. R. Paudel, C. W. Bark, Z. Huang, Ariando, E. Y. Tsymbal, G. Catalan, C. B. Eom, and A. Gruverman, Nano Lett. **15**, 3547 (2015).
[67]S. Das, B. Wang, Y. Cao, M. R. Cho, Y. Jae Shin, S. M. Yang, L. Wang, M. Kim, S. V. Kalinin, L. Q. Chen, and T. W. Noh, Nat. Commun. **8**, 615 (2017).
[68]S. Das, B. Wang, T. R. Paudel, S. M. Park, E. Y. Tsymbal, L. Q. Chen, D. Lee, and T. W. Noh, Nat. Commun. **10**, 537 (2019).
[69]S. M. Park, B. Wang, T. Paudel, S. Y. Park, S. Das, J. R. Kim, E. K. Ko, H. G. Lee, N. Park, L. Tao, D. Suh, E. Y. Tsymbal, L. Chen, T. W. Noh, and D. Lee, Nat. Commun. **11**, 2586 (2020).
[70]D. Lee, S. M. Yang, J. G. Yoon, and T. W. Noh, Nano Lett. **12**, 6436 (2012).
[71]M.-M. M. Yang, D. J. Kim, and M. Alexe, Science **360**, 904 (2018).
[72]M. M. Yang, A. N. Iqbal, J. J. P. Peters, A. M. Sanchez, and M. Alexe, Nat. Commun. **10**, 2791 (2019).

[73]K. Chu, B. K. Jang, J. H. Sung, Y. A. Shin, E. S. Lee, K. Song, J. H. Lee, C. S. Woo, S. J. Kim, S. Y. Choi, T. Y. Koo, Y. H. Kim, S. H. Oh, M. H. Jo, and C. H. Yang, Nat. Nanotechnol. **10**, 972 (2015).
[74]K. E. Kim, S. Jeong, K. Chu, J. H. Lee, G. Y. Kim, F. Xue, T. Y. Koo, L. Q. Chen, S. Y. Choi, R. Ramesh, and C. H. Yang, Nat. Commun. **9**, 403 (2018).
[75]L. J. Mcgilly, A. Kerelsky, N. R. Finney, K. Shapovalov, E. Shih, A. Ghiotto, Y. Zeng, S. L. Moore, W. Wu, Y. Bai, K. Watanabe, T. Taniguchi, M. Stengel, L. Zhou, J. Hone, X. Zhu, D. N. Basov, C. Dean, C. E. Dreyer, and A. N. Pasupathy, Nat. Nanotechnol. **15**, 580 (2020).
[76]V. Harbola, S. Crossley, S. S. Hong, D. Lu, Y. A. Birkhölzer, Y. Hikita, and H. Y. Hwang, Nano Lett. **21**, 2470 (2021).
[77]R. Roy, D. Nečas, and L. Zajíčková, Carbon **179**, 677 (2021).
[78]J. Jiang, Z. Chen, Y. Hu, Y. Xiang, L. Zhang, Y. Wang, G. C. Wang, and J. Shi, Nat. Nanotechnol. **16**, 894 (2021).
[79]D. Lu, D. J. Baek, S. S. Hong, L. F. Kourkoutis, Y. Hikita, and H. Y. Hwang, Nat. Mater. **15**, 1255 (2016).
[80]Y. Kim, S. S. Cruz, K. Lee, B. O. Alawode, C. Choi, Y. Song, J. M. Johnson, C. Heidelberger, W. Kong, S. Choi, K. Qiao, I. Almansouri, E. A. Fitzgerald, J. Kong, A. M. Kolpak, J. Hwang, and J. Kim, Nature **544**, 340 (2017).
[81]G. Dong, S. Li, M. Yao, Z. Zhou, Y. Q. Zhang, X. Han, Z. Luo, J. Yao, B. Peng, Z. Hu, H. Huang, T. Jia, J. Li, W. Ren, Z. G. Ye, X. Ding, J. Sun, C. W. Nan, L. Q. Chen, J. Li, and M. Liu, Science **366**, 475 (2019).
[82]D. Ji, S. Cai, T. R. Paudel, H. Sun, C. Zhang, L. Han, Y. Wei, Y. Zang, M. Gu, Y. Zhang, W. Gao, H. Huyan, W. Guo, D. Wu, Z. Gu, E. Y. Tsymbal, P. Wang, Y. Nie, and X. Pan, Nature **570**, 87 (2019).
[83]P. Gao, J. Britson, C. T. Nelson, J. R. Jokisaari, C. Duan, M. Trassin, S. H. Baek, H. Guo, L. Li, Y. Wang, Y. H. Chu, A. M. Minor, C. B. Eom, R. Ramesh, L. Q. Chen, and X. Pan, Nat. Commun. **5**, 3801 (2014).
[84]Q. Li, B. Wang, Q. He, P. Yu, L.-Q. Chen, V. K. Sergei, and J.-F. Li, Nano Lett. **21**, 445 (2021).
[85]J. Očenášek, H. Lu, C. W. Bark, C. B. Eom, J. Alcalá, G. Catalan, and A. Gruverman, Phys. Rev. B **92**, 035417 (2015).
[86]L. L. Ma, W. J. Chen, Y. L. Liu, B. Wang, and Y. Zheng, J. Phys.: Condens. Matter **31**, 145701 (2019).
[87]W. J. Chen, S. Yuan, L. L. Ma, Y. Ji, B. Wang, and Y. Zheng, RSC Adv. **8**, 4434 (2018).
[88]G. Li, X. Huang, J. Hu, and W. Zhang, Phys. Rev. B **95**, 144111 (2017).
[89]R. J. Zeches, M. D. Rossell, J. X. Zhang, A. J. Hatt, Q. He, C. H. Yang, A. Kumar, C. H. Wang, A. Melville, C. Adamo, G. Sheng, Y. H. Chu, J. F. Ihlefeld, R. Erni, C. Ederer, V. Gopalan, L. Q. Chen, D. G. Schldin, N. A. Spaldin, L. W. Martin, and R. Ramesh, Science **326**, 977 (2009).
[90]Y.-J. Li, J.-J. Wang, J.-C. Ye, X.-X. Ke, G.-Y. Gou, Y. Wei, F. Xue, J. Wang, C.-S. Wang, R.-C. Peng, X.-L. Deng, Y. Yang, X.-B. Ren, L.-Q. Chen, C.-W. Nan, and J.-X. Zhang, Adv. Funct. Mater. **25**, 3405 (2015).
[91]Y. Heo, B. K. Jang, S. J. Kim, C. H. Yang, and J. Seidel, Adv. Mater. **26**, 7568 (2014).
[92]Y. Cao, S. Yang, S. Jesse, I. Kravchenko, P. Yu, L.-Q. Chen, S. V. Kalinin, N. Balke, and Q. Li, Adv. Electron. Mater. **2**, 1600307 (2016).
[93]A. B. Naden, D. Edwards, S. M. Neumayer, J. G. M. Guy, B. J. Rodriguez, N. Bassiri-Gharb, and A. Kumar, Adv. Mater. Interfaces **5**, 1801019 (2018).
[94]A. N. Morozovska, E. A. Eliseev, A. K. Tagantsev, S. L. Bravina, L. Q. Chen, and S. V. Kalinin, Phys. Rev. B **83**, 195313 (2011).
[95]S. J. Kelly, Y. Kim, E. Eliseev, A. Morozovska, S. Jesse, M. D. Biegalski, J. F. Mitchell, H. Zheng, J. Aarts, I. Hwang, S. Oh, J. Sik Choi, T. Choi, B. Ho Park, S. V. Kalinin, and P. Maksymovych, Nanotechnology **25**, 475302 (2014).
[96]Y. Kim, S. J. Kelly, A. Morozovska, E. K. Rahani, E. Strelcov, E. Eliseev, S. Jesse, M. D. Biegalski, N. Balke, N. Benedek, D. Strukov, J. Aarts, I. Hwang, S. Oh, J. S. Choi, T. Choi, B. H. Park, V. B. Shenoy, P. Maksymovych, and S. V. Kalinin, Nano Lett. **13**, 4068 (2013).
[97]Y. Cao, A. Morozovska, and S. V. Kalinin, Phys. Rev. B **96**, 184109 (2017).
[98]A. Abdollahi, F. Vásquez-Sancho, and G. Catalan, Phys. Rev. Lett. **121**, 205502 (2018).
[99]J. Yvonnet, X. Chen, and P. Sharma, J. Appl. Mech. **87**, 111003 (2020).
[100]A. Biancoli, C. M. Fancher, J. L. Jones, and D. Damjanovic, Nat. Mater. **14**, 224 (2015).
[101]S. Hashemizadeh, A. Biancoli, and D. Damjanovic, J. Appl. Phys. **119**, 094105 (2016).
[102]H. Simons, A. B. Haugen, A. C. Jakobsen, S. Schmidt, F. Stöhr, M. Majkut, C. Detlefs, J. E. Daniels, D. Damjanovic, and H. F. Poulsen, Nat. Mater. **17**, 814 (2018).
[103]R. K. Vasudevan, N. Balke, P. Maksymovych, S. Jesse, and S. V. Kalinin, Appl. Phys. Rev. **4**, 21302 (2017).
[104]P. C. Wu, R. Huang, Y. H. Hsieh, B. Wang, M. Yen, S. Z. Ho, A. Kumamoto, C. Zhong, H. Song, Y. C. Chen, L. Q. Chen, C. G. Duan, Y. Ikuhara, and Y. H. Chu, NPG Asia Mater. **11**, 17 (2019).
[105]J. C. Agar, A. R. Damodaran, M. B. Okatan, J. Kacher, C. Gammer, R. K. Vasudevan, S. Pandya, L. R. Dedon, R. V. K. Mangalam, G. A. Velarde, S. Jesse, N. Balke, A. M. Minor, S. V. Kalinin, and L. W. Martin, Nat. Mater. **15**, 549 (2016).
[106]X. Wen, D. Li, K. Tan, Q. Deng, and S. Shen, Phys. Rev. Lett. **122**, 148001 (2018).
[107]E. A. Eliseev, A. N. Morozovska, A. V. Ievlev, N. Balke, P. Maksymovych, A. Tselev, and S. V. Kalinin, Appl. Phys. Lett. **104**, 232901 (2014).
[108]R. V. Wang, D. D. Fong, F. Jiang, M. J. Highland, P. H. Fuoss, C. Thompson, A. M. Kolpak, J. A. Eastman, S. K. Streiffer, A. M. Rappe, and G. B. Stephenson, Phys. Rev. Lett. **102**, 047601 (2009).
[109]Y. Cao and S. V. Kalinin, Phys. Rev. B **94**, 235444 (2016).
[110]A. S. Yurkov and A. K. Tagantsev, Appl. Phys. Lett. **108**, 022904 (2016).
[111]A. K. Tagantsev and A. S. Yurkov, J. Appl. Phys. **112**, 044103 (2012).
[112]W. Chen, J. Liu, L. Ma, L. Liu, G. L. Jiang, and Y. Zheng, J. Mech. Phys. Solids **111**, 43 (2018).
[113]E. Meirzadeh, D. V. Christensen, E. Makagon, H. Cohen, I. Rosenhek-Goldian, E. H. Morales, A. Bhowmik, J. M. G. Lastra, A. M. Rappe, D. Ehre, M. Lahav, N. Pryds, and I. Lubomirsky, Adv. Mater. **31**, 1904733 (2019).
[114]A. Y. Abid, N. Li, A. Arif, and P. Gao, arXiv:1811.02780 [Cond-Mat.Mtrl-Sci] (n.d.).
[115]C. A. Mizzi, A. Y. W. Lin, and L. D. Marks, Phys. Rev. Lett. **123**, 116103 (2019).
[116]B. N. J. Persson, Europhys. Lett. **129**, 10006 (2020).
[117]K. Y. Lee, S. K. Kim, J. H. Lee, D. Seol, M. K. Gupta, Y. Kim, and S. W. Kim, Adv. Funct. Mater. **26**, 3067 (2016).
[118]C. Yang, S. Xiao, J. C. Yang, X. Lu, Y. H. Chu, M. Zhou, F. Huang, and J. Zhu, Appl. Surf. Sci. **457**, 797 (2018).
[119]Y. T. Zhou and K. Y. Lee, J. Mech. Phys. Solids **59**, 1037 (2011).
[120]T. Jia, H. Kimura, Z. Cheng, H. Zhao, Y. H. Kim, M. Osada, T. Matsumoto, N. Shibata, and Y. Ikuhara, NPG Asia Mater. **9**, e349 (2017).
[121]T. Jia, H. Kimura, Z. Cheng, and H. Zhao, Sci. Rep. **6**, 31867 (2016).
[122]H. Y. Zhao, K. Cai, Z. X. Cheng, Z. Ma, H. Kimura, and T. Jia, J. Mater. Sci.: Mater. Electron. **27**, 5613 (2016).
[123]D. Lee, APL Mater. **8**, 090901 (2020).
[124]J. Bian, Y. Wang, R. Zhu, L. Wang, B. Yang, J. Wang, D. Zhang, C. Xu, T. Li, D. Viehland, and Y. Yang, ACS Appl. Mater. Interfaces **11**, 40758 (2019).
[125]Z. Chen, X. Wang, S. P. Ringer, and X. Liao, Phys. Rev. Lett. **117**, 027601 (2016).
[126]G. Vats, Ravikant, P. Schoenherr, A. Kumar, and J. Seidel, Adv. Electron. Mater. **6**, 2000523 (2020).
[127]P. Chen, X. Zhong, J. A. Zorn, M. Li, Y. Sun, A. Y. Abid, C. Ren, Y. Li, X. Li, X. Ma, J. Wang, K. Liu, Z. Xu, C. Tan, L. Chen, P. Gao, and X. Bai, Nat. Commun. **11**, 1840 (2020).
[128]X. Li, C. Tan, C. Liu, P. Gao, Y. Sun, P. Chen, M. Li, L. Liao, R. Zhu, J. Wang, Y. Zhao, L. Wang, Z. Xu, K. Liu, X. Zhong, J. Wang, and X. Bai, Proc. Natl. Acad. Sci. U.S.A. **117**, 18954 (2020).
[129]Y. Deng, C. Gammer, J. Ciston, P. Ercius, C. Ophus, K. Bustillo, C. Song, R. Zhang, D. Wu, Y. Du, Z. Chen, H. Dong, A. G. Khachaturyan, and A. M. Minor, Acta Mater. **181**, 501 (2019).
[130]D. Seol, B. Kim, and Y. Kim, Curr. Appl. Phys. **17**, 661 (2017).
[131]U. Celano, M. Popovici, K. Florent, S. Lavizzari, P. Favia, K. Paulussen, H. Bender, L. D. Piazza, J. Van Houdt, and W. Vandervorst, Nanoscale **10**, 8471 (2018).
[132]N. Balke, S. Jesse, A. N. Morozovska, E. Eliseev, D. W. Chung, Y. Kim, L. Adamczyk, R. E. García, N. Dudney, and S. V. Kalinin, Nat. Nanotechnol. **5**, 749 (2010).
[133]X. Chen, X. Tang, X. Chen, Y. Chen, X. Guo, H. Ge, and Q. Shen, Appl. Phys. Lett. **106**, 042903 (2015).

[134]J. Y. Jo, S. M. Yang, T. H. Kim, H. N. Lee, J. G. Yoon, S. Park, Y. Jo, M. H. Jung, and T. W. Noh, Phys. Rev. Lett. **102**, 045701 (2009).
[135]S. Liu, I. Grinberg, and A. M. Rappe, Nature **534**, 360 (2016).
[136]R. Waser, J. Am. Ceram. Soc. **74**, 1934 (1991).
[137]R. A. De Souza, Adv. Funct. Mater. **25**, 6326 (2015).
[138]H. I. Yoo, M. W. Chang, T. S. Oh, C. E. Lee, and K. D. Becker, J. Appl. Phys. **102**, 093701 (2007).
[139]Y. Gu, Z. Hong, J. Britson, and L. Q. Chen, Appl. Phys. Lett. **106**, 022904 (2015).
[140]A. N. Morozovska, E. A. Eliseev, Y. A. Genenko, I. S. Vorotiahin, M. V. Silibin, Y. Cao, Y. Kim, M. D. Glinchuk, and S. V. Kalinin, Phys. Rev. B **94**, 174101 (2016).
[141]B. Wang, H. Lu, C. W. Bark, C.-B. Eom, A. Gruverman, and L.-Q. Chen, Acta Mater. **193**, 151 (2020).
[142]B. Cappella and G. Dietler, Surf. Sci. Rep. **34**, 1 (1999).
[143]M. J. Higgins, R. Proksch, J. E. Sader, M. Polcik, S. Mc Endoo, J. P. Cleveland, and S. P. Jarvis, Rev. Sci. Instrum. **77**, 013701 (2006).
[144]J. P. Cleveland, S. Manne, D. Bocek, and P. K. Hansma, Rev. Sci. Instrum. **64**, 403 (1993).
[145]J. E. Sader, J. W. M. Chon, and P. Mulvaney, Rev. Sci. Instrum. **70**, 3967 (1999).
[146]J. L. Hutter and J. Bechhoefer, Rev. Sci. Instrum. **64**, 1868 (1993).
[147]S. J. Kennedy, D. G. Cole, and R. L. Clark, Rev. Sci. Instrum. **80**, 125103 (2009).
[148]R. Proksch, T. E. Schäffer, J. P. Cleveland, R. C. Callahan, and M. B. Viani, Nanotechnology **15**, 1344 (2004).
[149]Y. Song, S. Wu, L. Xu, and X. Fu, Sensors (Switzerland) **15**, 5865 (2015).
[150]C. Yildirim, P. Cook, C. Detlefs, H. Simons, and H. F. Poulsen, MRS Bull. **45**, 277 (2020).
[151]A. C. Fischer-Cripps, E. F. Gloyna, and W. H. Hart, *Introduction to Contact Mechanics* (Springer, 2000).
[152]A. E. Giannakopoulos and S. Suresh, Acta Mater. **47**, 2153 (1999).
[153]W. Chen and H. Ding, Acta Mech. Solida Sin. **12**, 114 (1999).
[154]E. Karapetian, E. Sevostianov, and M. Kachanov, Philos. Mag. B **80**, 331 (2000).
[155]E. Karapetian, M. Kachanov, and S. V. Kalinin, Philos. Mag. **85**, 1017 (2005).
[156]F. Yang, Int. J. Appl. Electromagn. Mech. **43**, 347 (2013).
[157]F. Yang, Mater. Sci. Eng. A **358**, 226 (2003).
[158]J. H. Wang, C. Q. Chen, and T. J. Lu, J. Mech. Phys. Solids **56**, 3331 (2008).
[159]Y. F. Wu, H. Y. Yu, and W. Q. Chen, Int. J. Solids Struct. **49**, 95 (2012).
[160]J. S. Wang, X. J. Zheng, H. Zheng, Z. Zhu, and S. T. Song, Appl. Surf. Sci. **256**, 5998 (2010).
[161]S. V. Kalinin, E. Karapetian, and M. Kachanov, Phys. Rev. B **70**, 184101 (2004).
[162]F. Yang, J. Appl. Phys. **103**, 074115 (2008).
[163]B. L. Wang and J. C. Han, Arch. Appl. Mech. **76**, 367 (2006).
[164]K. Pan, Y. Y. Liu, S. H. Xie, Y. M. Liu, and J. Y. Li, Acta Mater. **61**, 7020 (2013).
[165]X. Li and M. Wang, J. Elast. **84**, 153 (2006).
[166]J. H. Wang and C. Q. Chen, Int. J. Solids Struct. **48**, 2743 (2011).
[167]B. B. L. Wang, J. C. Han, S. Y. Du, H. Y. Zhang, and Y. G. Sun, Int. J. Solids Struct. **45**, 6384 (2008).
[168]J. Li, W. Xiong, X. Huang, W. Chen, and Y. Zheng, J. Appl. Phys. **129**, 244105 (2021).
[169]Y.-T. Zhou and K. Y. Lee, Eur. J. Mech. A. Solids **35**, 22 (2012).
[170]J. Ma, L. L. Ke, and Y. S. Wang, Appl. Math. Modell. **38**, 5471 (2014).
[171]A. Makagon, M. Kachanov, S. V. Kalinin, and E. Karapetian, Phys. Rev. B **76**, 064115 (2007).
[172]L. Rodríguez-Tembleque, A. Sáez, and M. H. Aliabadi, Int. J. Eng. Sci. **107**, 36 (2016).
[173]Y. T. Zhou and K. Y. Lee, Mech. Mater. **69**, 237 (2014).
[174]L. Q. Chen, Annu. Rev. Mater. Sci. **32**, 113 (2002).
[175]A. N. Morozovska, E. A. Eliseev, S. L. Bravina, and S. V. Kalinin, J. Appl. Phys. **110**, 052011 (2011).
[176]A. G. Khachaturyan, *Theory of Structural Transformations in Solids* (John Wiley and Sons, New York, 1983).
[177]L.-Q. Chen, J. Am. Ceram. Soc. **91**, 1835 (2008).
[178]J.-J. Wang, B. Wang, and L.-Q. Chen, Annu. Rev. Mater. Res. **49**, 127 (2019).
[179]T. Yang, B. Wang, J.-M. Hu, and L.-Q. Chen, Phys. Rev. Lett. **124**, 107601 (2020).
[180]W. Xiong, J. Liu, L. Ma, W. Chen, and Y. Zheng, J. Appl. Phys. **128**, 014102 (2020).
[181]H. X. Song, L. L. Ke, J. Su, J. Yang, S. Kitipornchai, and Y. S. Wang, Int. J. Solids Struct. **185–186**, 380 (2020).
[182]C. Qi and X. Wang, J. Appl. Phys. **129**, 094101 (2021).
[183]F. Wu, X. Y. Li, R. F. Zheng, and G. Z. Kang, Int. J. Eng. Sci. **134**, 77 (2019).
[184]F. Jin, S. Yan, X. Guo, and X. Wang, Mech. Mater. **129**, 189 (2019).
[185]W. Liu, F. Deng, S. Xie, S. Shen, and J. Li, J. Mech. Phys. Solids **142**, 104020 (2020).
[186]S. S. Hong, M. Gu, M. Verma, V. Harbola, B. Y. Wang, D. Lu, A. Vailionis, Y. Hikita, R. Pentcheva, J. M. Rondinelli, and H. Y. Hwang, Science **368**, 71 (2020).
[187]D. Pesquera, E. Parsonnet, A. Qualls, R. Xu, A. J. Gubser, J. Kim, Y. Jiang, G. Velarde, Y. L. Huang, H. Y. Hwang, R. Ramesh, and L. W. Martin, Adv. Mater. **32**, 2003780 (2020).
[188]H. S. Kum, H. Lee, S. Kim, S. Lindemann, W. Kong, K. Qiao, P. Chen, J. Irwin, J. H. Lee, S. Xie, S. Subramanian, J. Shim, S. H. Bae, C. Choi, L. Ranno, S. Seo, S. Lee, J. Bauer, H. Li, K. Lee, J. A. Robinson, C. A. Ross, D. G. Schlom, M. S. Rzchowski, C. B. Eom, and J. Kim, Nature **578**, 75 (2020).
[189]Q. Deng, L. Liu, and P. Sharma, Phys. Rev. E **90**, 012603 (2014).
[190]H. Elangovan, M. Barzilay, S. Seremi, N. Cohen, Y. Jiang, L. W. Martin, and Y. Ivry, ACS Nano **14**, 5053 (2020).
[191]T. Q. Thai, T. Rabczuk, and X. Zhuang, Comput. Methods Appl. Mech. Eng. **341**, 718 (2018).
[192]D. Codony, P. Gupta, O. Marco, and I. Arias, J. Mech. Phys. Solids **146**, 104182 (2021).
[193]H. Lu, B. Wang, T. Li, A. Lipatov, H. Lee, A. Rajapitamahuni, R. Xu, X. Hong, S. Farokhipoor, L. W. Martin, C.-B. Eom, L.-Q. Chen, A. Sinitskii, and A. Gruverman, Nano Lett. **16**, 6460 (2016).
[194]L. Chen, Z. Cheng, W. Xu, X. Meng, G. Yuan, and J. Liu, Sci. Rep. **6**, 19092 (2016).
[195]D. J. Kim, T. R. Paudel, H. Lu, J. D. Burton, J. G. Connell, E. Y. Tsymbal, S. S. A. Seo, and A. Gruverman, Adv. Mater. **26**, 7660 (2014).
[196]M. H. Yusuf, A. Gura, X. Du, and M. Dawber, 2D Mater. **4**, 021022 (2017).
[197]S. Yun, K. Song, K. Chu, S. Y. Hwang, G. Y. Kim, J. Seo, C. S. Woo, S. Y. Choi, and C. H. Yang, Nat. Commun. **11**, 4898 (2020).
[198]C. Wang, X. Ke, J. Wang, R. Liang, Z. Luo, Y. Tian, D. Yi, Q. Zhang, J. Wang, X.-F. Han, G. Van Tendeloo, L.-Q. Chen, C.-W. Nan, R. Ramesh, and J. Zhang, Nat. Commun. **7**, 10636 (2016).
[199]B. Chu, W. Zhu, N. Li, and L. E. Cross, J. Appl. Phys. **106**, 104109 (2009).
[200]W. Zhu, J. Y. Fu, N. Li, and L. Cross, Appl. Phys. Lett. **89**, 192904 (2006).
[201]Y. Shi, Y. Guo, X. Wang, A. J. Princep, D. Khalyavin, P. Manuel, Y. Michiue, A. Sato, K. Tsuda, S. Yu, M. Arai, Y. Shirako, M. Akaogi, N. Wang, K. Yamaura, and A. T. Boothroyd, Nat. Mater. **12**, 1024 (2013).
[202]A. S. Yurkov and P. V. Yudin, J. Appl. Phys. **129**, 195108 (2021).
[203]J. W. Hong, D. S. Kahng, J. C. Shin, H. J. Kim, and Z. G. Khim, J. Vac. Sci. Technol. B **16**, 2942 (1998).
[204]F. Zhang, W.-M. Jiang, C.-J. Li, Y. Jin, Z. Wang, J.-C. Nie, and J.-y. Dai, ACS Appl. Electron. Mater. **2**, 1861 (2020).
[205]D. Seol, S. M. Yang, S. Jesse, M. Choi, I. Hwang, T. Choi, B. H. Park, S. V. Kalinin, and Y. Kim, Nanotechnology **29**, 275709 (2018).
[206]M. Y. Zhuravlev, R. F. Sabirianov, S. S. Jaswal, and E. Y. Tsymbal, Phys. Rev. Lett. **94**, 246802 (2005).
[207]E. Y. Tsymbal and H. Kohlstedt, Science **313**, 181 (2006).
[208]V. Garcia, S. Fusil, K. Bouzehouane, S. Enouz-Vedrenne, N. D. Mathur, A. Barthélémy, and M. Bibes, Nature **460**, 81 (2009).
[209]Y. W. Yin, J. D. Burton, Y.-M. Kim, A. Y. Borisevich, S. J. Pennycook, S. M. Yang, T. W. Noh, A. Gruverman, X. G. Li, E. Y. Tsymbal, and Q. Li, Nat. Mater. **12**, 397 (2013).
[210]V. Garcia and M. Bibes, Nat. Commun. **5**, 4289 (2014).
[211]P. Maksymovych, S. Jesse, P. Yu, R. Ramesh, A. P. Baddorf, and S. V. Kalininl, Science **324**, 1421 (2009).
[212]H. Lu, D. J. Kim, C. W. Bark, S. Ryu, C. B. Eom, E. Y. Tsymbal, and A. Gruverman, Nano Lett. **12**, 6289 (2012).

[213]Y. Wang, K. Zhao, X. Shi, G. Li, G. Xie, X. Lai, J. Ni, and L. Zhang, Sci. Rep. **5**, 10841 (2015).
[214]C. Zener, Proc. R. Soc. London, Ser. A **145**, 523 (1934).
[215]G. Singh-Bhalla, C. Bell, J. Ravichandran, W. Siemons, Y. Hikita, S. Salahuddin, A. F. Hebard, H. Y. Hwang, and R. Ramesh, Nat. Phys. **7**, 80 (2011).
[216]X. Xu, Y. Wang, F. T. Huang, K. Du, E. A. Nowadnick, and S. W. Cheong, Adv. Funct. Mater. **30**, 2003623 (2020).
[217]S. Li and T. Birol, NPJ Comput. Mater. **6**, 168 (2020).
[218]X. Xu, F. T. Huang, Y. Qi, S. Singh, K. M. Rabe, D. Obeysekera, J. Yang, M. W. Chu, and S. W. Cheong, Nat. Mater. **20**, 826 (2021).
[219]E. I. Rashba, Sov. Phys. Solid State **2**, 1109 (1960).
[220]L. P. Gor'kov and E. I. Rashba, Phys. Rev. Lett. **87**, 037004 (2001).
[221]D. D. Awschalom and M. E. Flatté, Nat. Phys. **3**, 153 (2007).
[222]D. Awschalom and N. Samarth, Physics **2**, 50 (2009).
[223]E. Bauer and M. Sigrist, *Non-Centrosymmetric Superconductors: Introduction and Overview* (Springer, 2012).
[224]T. Ideue, K. Hamamoto, S. Koshikawa, M. Ezawa, S. Shimizu, Y. Kaneko, Y. Tokura, N. Nagaosa, and Y. Iwasa, Nat. Phys. **13**, 578 (2017).
[225]L. Wang, Q. Feng, Y. Kim, R. Kim, K. H. Lee, S. D. Pollard, Y. J. Shin, H. Zhou, W. Peng, D. Lee, W. Meng, H. Yang, J. H. Han, M. Kim, Q. Lu, and T. W. Noh, Nat. Mater. **17**, 1087 (2018).
[226]C. Lee, X. Wei, J. W. Kysar, and J. Hone, Science **321**, 385 (2008).
[227]S. Y. Zhou, G. Gweon, A. V. Fedorov, P. N. First, W. A. de Heer, D. Lee, A. H. C. Neto, and A. Lanzara, Nat. Mater. **6**, 770 (2007).
[228]R. Balog, B. Jørgensen, L. Nilsson, M. Andersen, E. Rienks, M. Bianchi, M. Fanetti, E. Lægsgaard, A. Baraldi, S. Lizzit, Z. Sljivancanin, F. Besenbacher, B. Hammer, T. G. Pedersen, P. Hofmann, and L. Hornekær, Nat. Mater. **9**, 315 (2010).
[229]M. Dvorak, W. Oswald, and Z. Wu, Sci. Rep. **3**, 2289 (2013).
[230]M. Yankowitz, J. Jung, E. Laksono, N. Leconte, B. L. Chittari, K. Watanabe, T. Taniguchi, S. Adam, D. Graf, and C. R. Dean, Nature **557**, 404 (2018).
[231]Y. Liu, N. O. Weiss, X. Duan, H. Cheng, Y. Huang, and X. Duan, Nat. Rev. Mater. **1**, 16042 (2016).
[232]H. J. Mamin, R. P. Ried, B. D. Terris, and D. Rugar, Proc. IEEE **87**, 1014 (1999).